Lateralization of Directional Brain-Heart Information Transfer during Visual Emotional Elicitation

Alberto Greco*,c, Luca Faes*, Vincenzo Catrambone, Riccardo Barbieri,

Enzo Pasquale Scilingo, and Gaetano Valenza

Abstract

Previous studies have characterized the physiological interactions between central nervous system (brain) and peripheral cardiovascular system (heart) during affective elicitation in the healthy, however questions related to the directionality of this functional interplay have been gaining less attention from the scientific community. Here, we explore brain-heart interactions during visual emotional elicitation in healthy subjects using measures of Granger causality (GC), a widely used descriptor of causal influences between two dynamical systems. The proposed approach inferences causality between instantaneous cardio-vagal dynamics estimated from inhomogeneous point-process models of the heartbeat, and high-density electroencephalogram (EEG) dynamics in 22 healthy subjects who underwent pleasant/unpleasant affective elicitation by watching pictures from the International Affective Picture System database. Particularly, we calculated the GC indexes between the EEG spectrogram in the canonical θ, α, β and γ bands, and both the instantaneous mean heart rate and its continuous parasympathetic modulations (i.e., the instantaneous HF power). Thus, we looked for significant statistical differences among GC values estimated during resting state, neutral elicitation, and pleasant/unpleasant arousing elicitation. As compared with resting state, coupling strength increases significantly in the left hemisphere during positive stimuli, and in the right hemisphere during negative stimuli. Our results further reveal a correlation between emotional valence and lateralization of the dynamical information transfer going from-brain-to-heart, mainly localized in the prefrontal, somatosensory, and posterior cortices, and of the information transfer from-heart-to-brain, mainly reflected into the fronto-parietal cortex oscillations in the γ band (30−45Hz).

c Corresponding Author: a.greco@centropiaggio.unipi.it.

A. Greco, V. Catrambone, EP Scilingo, and G. Valenza are with the Computational Physiology and Biomedical Instruments group at the Bioengineering and Robotics Research Center E. Piaggio and Department of Information Engineering, University of Pisa, Pisa, Italy.

L. Faes is with the Department of Energy, Information engineering and Mathematical models (DEIM), University of Palermo, Palermo, Italy.

R. Barbieri is with the Department of Electronics, Informatics and Bioengineering, Politecnico di Milano, Milano, Italy.

* These Authors equally contributed to this work

I. Introduction

A long-lasting scientific debate about the physiological origin of emotions is currently open: are emotions elicited by peripheral stimuli and responses (i.e., unconscious reactions mediated by the autonomic nervous system (ANS)) or are they ultimately created within specific brain areas (i.e., from an entirely cognitive process) (16)?

The dynamic physiological interactions between central nervous system (brain) and peripheral cardiovascular system (heart) have been gaining relevant attention from the scientific community in the last decade. The nature of these interactions is deeply connected to the switching mechanisms between healthy and pathological states, as well as between stress, emotions, and other homeostatic regulations. As a matter of fact, emotional processing and regulation are known to significantly alter peripheral physiological responses mediated by the ANS (15, 19), although this vagally-mediated regulation deeply involves also the limbic system and the prefrontal cortex (16, 32, 46, 72). Here, we start from the hypothesis that both brain and heart have a crucial role in the dynamical regulation and processing of emotions, studying the causal links between these physiological systems probed in the healthy by means of high-resolution electroencephalography (EEG) and heart rate variability (HRV). Our hypothesis relies on recent evidences demonstrating that the emotional response takes root in the dynamical interplay between the brain and heart (17, 19, 32, 78, 80).

Anatomically, the heart has extensive efferent and afferent neural connections with the brain that may be thought as constituting the physiological foundation of a “brain-heart” emotional pathway (17). Cardiac dynamics result from the synergistic action of the two ANS branches, the sympathetic and parasympathetic (vagus) nervous systems, whose regulation involves complex cortical, subcortical, and medullary signaling (55). To this extent, HRV time series directly result from the balancing effect of sympathovagal activity on cardiovascular control (58). From HRV signal processing in the frequency domain, the power spectral density within the 0.15-0.4 Hz range (the so-called high-frequency, HF, band) is known to be mediated by parasympathetic nerve activity (33, 58), whereas the power in the 0.04−0.15 Hz range (i.e., low-frequency, LF, band) is thought to result from both parasympathetic and sympathetic activity (64).

From the brain side, the insular cortex, which controls the parasympathetic and the sympathetic tones (73), plays also a prominent role in emotional processing, as documented by numerous functional neuroimaging and neuropsychological investigations (37, 41). Specifically, the anterior insular cortex, which is part of the limbic system, is increasingly studied for its role in emotional awareness (18, 84). Not surprisingly, patients with insular damage after a stroke exhibit cardiovascular instability and are prone to autonomic alterations and even sudden cardiovascular death (53, 54). Furthermore, the medial prefrontal cortex, besides contributing to several cognitive functions, is involved in the regulation of cardiovascular functions (14). Importantly, strong emotion and mental stress, which significantly affect the activity of the prefrontal cortex, are

recognized as playing a significant role in severe cardiac arrhythmias (71). On the other side, cardiac afferent inputs significantly influence the activity of brain areas that are involved in perceptual and cognitive processing, as well as in an emotional experience, e.g., the thalamus, hypothalamus, and amygdala (12, 27, 47). Note that, exemplarily, neural activity in the amygdala are synchronized with the cardiac cycle (29).

Recently, we have analyzed brain-heart interactions during visual emotion elicitation in healthy subjects using the maximal information coefficient throughout different levels of arousal at different levels of valence (78). Note that, following the Circumplex Model of Affect (CMA) (57), a specific emotion can be seen as a result from the combination of a valence level, identified by the perceptual degree of pleasantness or unpleasantness, and arousal level, identified by the perceptual degree of intensity. Although successful in the characterization of the information shared by heart and brain during emotional perception, our previous endeavor (78) left the question open about how information is transferred dynamically along the two directions of the brain-heart axis.

To fill this gap, in this study we employ Granger Causality (GC) to characterize cortical influences on heartbeat dynamics, and vice-versa, during visual emotional perception in healthy subjects. GC is a very popular and well-principled tool for assessing directional interactions from time series data (10, 31, 56). We show experimental results on GC for the directional brain-heart interplay during visual emotional perception using data gathered from twenty-two healthy subjects who were emotionally elicited through passive viewing of standardized pictures from the International Affective Picture System (IAPS) (42) database. These images have been widely employed in recent scientific studies and are fully characterized in terms of valence and arousal levels (42). Our physiological inference is mainly focused on the functional interplay between cortical and parasympathetic dynamics. To this extent, vagal activity is derived from a spectral analysis of HRV series given a time-frequency analysis of respiratory dynamics (58).

Preliminary findings of this research were recently reported in (23). Methodological details, as well as extensive Results, and Discussion and Conclusions follow below.

II. MATERIALS AND METHODS

II.A. Acquisition set-up and experimental protocol

The experimental paradigm has been extensively described in (76, 78, 79). A brief summary is reported below.

Participants: Twenty-two healthy volunteers (11 females) aged from 21 to 24 were recruited at the University of Pisa. All subjects were asked to fill out a Patient Health Questionnaire^{TM} (PHQ-9), which is a self-administered questionnaire for the diagnosis of mental health disorders, e.g., depression. Subjects who obtained a score below a threshold of 5 were enrolled in the

experiment (39). The study was approved by the local ethical committee, and an informed consent was signed by all volunteers. All procedures performed in this study were in accordance with the ethical standards of the institutional and/or national research committee and with the 1964 Helsinki declaration and its later amendments or comparable ethical standards. This protocol was approved by the Ethical Committee of the University of Pisa-Pisa University Hospital, Pisa (Italy).

Stimuli: The experimental protocol uses the IAPS database (42) relying on CMA theory (57) for the emotional characterization. The IAPS database is a large collection of images, which are standardized with a specific affective rating expressed in terms of arousal and valence. We selected five groups of images along the arousal dimension (A1, A2, A3, A4, and A5) comprising pleasant and unpleasant elicitations of several valence degrees. To this extent, we can distinguish neutral (N), arousing positive (ARP), and arousing negative (ARN) elicitations in addition to a resting state (R).

Procedure: The aforementioned sequence of IAPS images was projected onto a PC screen. The slide-show comprised 9 sessions of 20 images each. The images were clustered according to their arousal scores into 4 groups. A1 (Mean (M) = *3.58*, Standard Deviation (SD) = *.30*), A2 (M = 4.60, SD = *.31*), A3 (M = *5.55*, SD = *.28*), A4 (M = *6.50*, SD = *.33*). Each arousal group included 10 pictures with positive valence (i.e. pleasant) and 10 pictures with negative valence (i.e., unpleasant), and was alternated between two neutral sessions (N, comprised of 6 pictures each, with *M= 2.81*, *SD=.24*). Every picture was shown for 10s.

Data acquisition: Throughout the experimental sessions, brain signals were acquired through the Geodesic EEG Systems 300 from the Electrical Geodesics, Inc. The Geodesic net included 128 electrodes and had the advantages to be easy to use and comfortable. The mastoid signal average was used as a reference. The ECG was recorded using a BIOPAC MP150 physiological acquisition system through Ag/AgCl surface electrodes positioned on the participant's chest in a modified lead II configuration. In addition, a second input channel of the BIOPAC MP150 system was used to record the respiration activity through a thoracic piezoresistive band. All signals were digitized at 500 Hz. The experiment was performed in strictly controlled conditions. The room was illuminated by a white neon lighting, with a power of 50 lumens, equally distributed. Subjects were asked to sit on a comfortable chair at a fixed distance of 70 cm from the screen configured with maximum brightness.

II.B. EEG processing

The EEG data processing was mostly performed using the MATLAB toolbox, EEGLAB (21).

The pre-processing included the four following steps: data filtering, head/body movement artifact detection and removal, eye blink artifact detection and removal and interpolation of corrupted channels.

1) Data filtering: A 6^{th}-order Butterworth infinite impulse response bandpass filter with cut-off frequencies of 1-45 Hz was

applied on the raw EEG signals to reduce the out-of-band noise.

2) Head/body detection and removal: An algorithm for the detection of artifact due to head and/or body movements was implemented (78). First, the EEG signals were divided into 4s-epochs. Then, the distribution of epoch amplitudes was computed and the epochs above the 95th percentile threshold was excluded from the following analyses. This automatic process was further validated by a visual inspection.

3) Eye artifacts detection and removal: Independent component analysis (ICA) was applied to EEG signals to separate neural activity from blink artifacts. ICA is a common method for solving the blind source separation problem which imposes a statistical independence to the output pairs. The Independent component containing ocular artifacts were discarded after a visual inspection (35). Eye-artifact-free EEG signals were obtained by projecting selected non-artifactual ICA components back (35).

4) Interpolation of corrupted channels: Corrupted channels can be defined (21) as EEG signals with several unexpected events and presence of high-frequency noise. In order to detect the EEG-corrupted channels, we built a 3D-space whose axes were the second, the third, and the forth central moments. The good EEG channels were commonly clustered together, whereas the corrupted ones drifted apart in different directions according to their artefactual nature (77). Therefore, in the 3D space, we computed the channel central moment distribution and we measured the distance of each channel from the distribution centroid. The channels exceeding a threshold value by twice the interquartile range for at least one dimension were replaced with interpolated data. Moreover, in this case the process was further validated by a visual inspection.

5) Spectral Analysis: Spectral analysis was performed estimating the power spectral density (PSD) of each channel by means of the Welch's method. Specifically, the squared magnitude of the fast Fourier transform was averaged across moving and 75%-overlapping time windows of 4 seconds. The overlap of 75% was chosen to decrease the PSD variance. After the PSD estimation, the power spectra were computed within the classical frequency bandwidths of θ [4−8 Hz), α [8−14 Hz), β [14−32 Hz) and γ ($\geq$ 32 Hz) (77).

II.C. Instantaneous Heart Rate Variability Processing

The ECG signal was analyzed off-line to extract the RR intervals. Erroneous and ectopic beats were corrected by a previously developed algorithm, based on the point-process modeling (77). Starting from the RR interval series, instantaneous cardiovascular dynamics with a 5ms resolution was estimated through point-process modeling (see details in (75, 77)). An inverse-Gaussian probability density function is associated with each heartbeat event (i.e., R-peaks from the ECG). Each of these functions is parametrized in its shape parameter and mean value, which is modeled as a linear combination of the past RR intervals. A local maximum likelihood method (78) was used to calculate the model parameter within a sliding window of $W = 70s$, obtaining time-varying estimates every 5ms. The model goodness-of-fit is based on the Kolmogorov-Smirnov (KS)

test and associated KS statistics (see details in (78)). Autocorrelation plots were considered to test the independence of the model-transformed intervals (78). The instantaneous mean RR interval and the HF power spectrum estimated by point-process modeling, subsampled synchronously with the EEG power time series, were taken as realizations of from-heart dynamics η onto the brain.

II.D. Time-frequency analysis of respiratory dynamics

The respiratory signal was processed to identify the fundamental respiratory frequency over time. Specifically, a time-frequency analysis was performed by applying the short-time-Fourier-transform to the respiration signal recorded throughout the experiment. We used a sliding Hamming window with a length of 1 minute, to allow for necessary frequency resolution, and 90 % of overlap, to smooth the time-frequency representation.

II.E. Granger Causality Analysis

The values of EEG spectral power computed in the four canonical bands (θ, α, β, and γ) were obtained with a temporal spacing of one second. Therefore, to synchronize cardiovascular and brain time series, the instantaneous series of mean HRV and HF spectral power were averaged within non-overlapped time windows of one second. The time series obtained in this way were considered separately for each of the four experimental conditions (R, N, ARP, ARN). Then, taking only the blocks of data belonging to the same condition, each series was detrended using a zero-phase high-pass filter with .015 Hz cut-off frequency, and normalized to zero-mean and unit variance.

The four EEG power time series calculated for each electrode, in each experimental condition (R, N, ARP, ARN) were considered as a realization of a 4-dimensional stochastic process descriptive of the brain dynamics, $\mathbf{\Phi} = \{\theta, \alpha, \beta, \gamma\}$. The heartbeat dynamics measured in synchrony with the brain dynamics were described by means of a scalar stochastic process η, obtained taking alternatively the time series of mean HRV (η_μ) or the time series of the HF power (η_{HF}); these alternative choices of the cardiac process were made to allow interpreting its dynamics either as an index of the overall HRV (η_μ), or as an index of vagal modulation (η_{HF}).

Then, Granger causality (GC) analysis was performed considering the M-dimensional stochastic process $\mathbf{X} = [X_1, \dots, X_5]$= $[\mathbf{\Phi}, \eta]$ (here, M = 5). Assuming the scalar process X_j as the target and the (possibly vector) process $\mathbf{X}_i$ as the driver ($i,j \in \{1,\dots,M\}$, $i \neq j$), GC quantifies, within a linear prediction framework, the amount of information transferred from $\mathbf{X}_i$ to X_j intended as the extent to which the knowledge of the past states of the driver, $\mathbf{X}_{i,j}^- = \left[\mathbf{X}_{i,t-1}, \mathbf{X}_{i,t-2}, \dots\right]$, improves the prediction of the present state of the target, $X_{j,t}$, above and beyond the extent to which $X_{j,t}$ is predicted by its own past states, $X_{i,j}^- = \left[X_{i,t-1}, X_{i,t-2}, \dots\right]$. This definition is quantified using two nested linear prediction models, the first

performing the regression of $X_{i,j}$ on $X_{i,j}^{-}$ and the second performing the regression of $X_{i,j}$ on $[\mathbf{X}_{i,j}^{-}, \mathbf{X}_{i,j}^{-}]$.These two regressions yield the prediction errors $W_{j|j,t}$ and $W_{j|ij,t}$whose variances $\sigma_{j|j}^2$ and $\sigma_{j|ij}^2$ are combined to yield a *Granger Causality Index* (GCI) from $\mathbf{X}_i$ to X_j as (3):

$$F_{i\to j} = \log\left(\frac{\sigma_{j|j}^2}{\sigma_{j|ij}^2}\right) \quad (1)$$

In this study, GCI was computed from the state-space representation of the process **X** (3). Compared with the classical vector autoregressive (VAR) description of full and restricted models, the state-space description has the advantage of providing a closed-form representation of the sub-models that result when the driver is omitted. This allows computing multiple prediction error variances without repeating model identification, and ultimately results in a dramatic reduction of the estimation bias. Details on computation of the partial variances from the parameters of a state-space model can be found in (4, 25).

The GC analysis described above was repeated two times considering either η_μ or η_{HF} as the cardiovascular process $\eta = X_5$, together with $\mathbf{\Phi} = \{\theta, \alpha, \beta, \gamma\} = [X_1, \ldots, X_4]$ as the brain process. Practical estimation of GC was performed first identifying the VAR model fitting the brain and cardiovascular time series measured for each condition and each of the 128 EEG channels, and then passing the estimated VAR parameters to state-space analysis. VAR identification was performed through the standard least squares method, drawing the observations of the present and past values of the five processes from the data blocks relevant to the analyzed condition. The number of past samples used in the identification (VAR model order) was set according to the Akaike Information Criterion. The estimated VAR model parameters were exploited in the state-space framework to compute all the prediction error variances needed for the computation of GCI. Specifically, Eq. 1 was used to compute the information transferred jointly from all brain processes to the cardiovascular system ($F_{\Phi\to\eta_y}$), and the information transferred from the heart process to each assigned brain process ($F_{\eta_y\to\Phi_x}$), where y and x correspond to one of the two cardiovascular measures (μ and HF), and to one of the four EEG bandwidths (θ, α, β, or γ), respectively. Moreover, the statistical significance of each GC measure was assessed by using the traditional Fisher F-test, under the null hypothesis of absence of GC (10). For each subject, each GC was detected as statistically significant if the F statistic was greater than the critical value from a Fisher distribution computed for a significance level of .05.

II.F. Statistical Comparisons between the four different experimental conditions (R, N, ARN, ARP)

For both brain-to-heart and heart-to-brain interactions, we assessed the significant statistical differences among the four different experimental conditions (R, N, ARN, ARP). Specifically, for each of the six pairs of experimental conditions, the given measure of information transfer was compared using a Wilcoxon signed-rank test with Bonferroni correction for multiple

comparisons. A p-value lower than 0.05 was considered as statistically significant.

II.G. Statistical assessment of the lateralization effect

To evaluate the tendency of a brain hemisphere to be specialized for affective afferent/efferent brain-heart interplay, we tested whether the proportions of significant electrodes, resulted from the pairwise comparisons among R, N, ARN, ARP, were statistically different between the right and left hemisphere using chi-squared tests.

III. Experimental Results

On average, the length of the sets of data analyzed in the various conditions were 485 sec during R, 247 sec during N, 273 sec during ARN, and 270 sec during ARP. Of note, we tested for possible interactions for all different durations of the time series, finding no significant interactions. The average VAR model order selected by the AIC criterion is 4.6, 3.6, 4.0 and 3.9 during R, N, ARN, and ARP, respectively.

As detailed in (78), all EEG recordings show more than 90% of artifact-free epochs. No subjects were discarded and, therefore, the results described in this section come from data gathered from all 22 volunteers. The optimal model order for point-process models of heartbeat dynamics was found to be $p = 7$, with KS distances never above .051 (78).

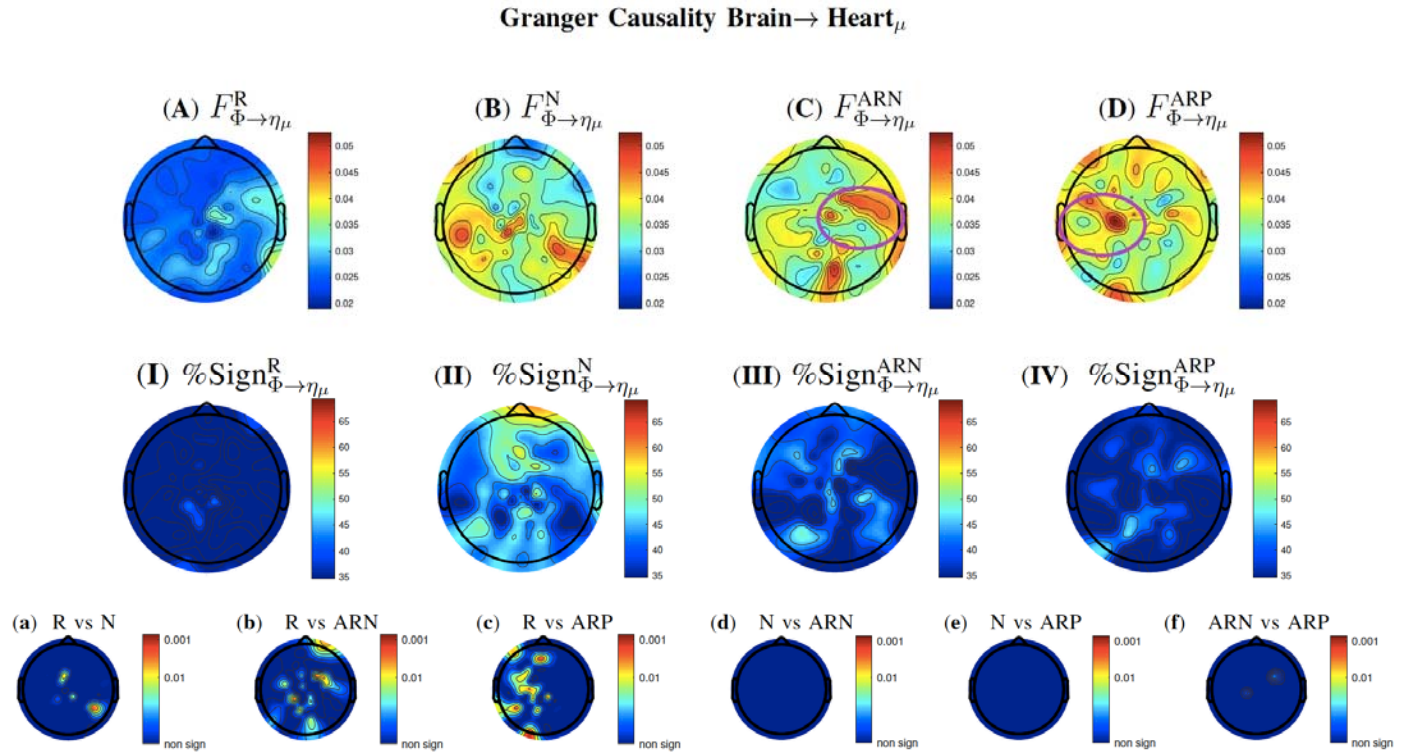

Fig. 1. Topographic maps in the first-row panel show Granger Causality values from EEG power spectrum computed in all frequency band to instantaneous heart rate dynamics ($F_{\Phi\to\eta_\mu}$). The four maps correspond to the four experimental conditions (R: rest; N: Neutral elicitation; ARN: Arousing elicitation with negative valence; ARP: Arousing elicitation with positive valence). In the second row, topographic maps represent percentage of subjects showing a significant GCI according to the F-test results for each electrode and experimental condition. In the third row, topographic maps give a graphical representation of post-hoc statistical results. The six maps correspond to the six pairwise comparisons among the four experimental conditions. Color scale shows p-values corrected for multiple comparisons.

Results from the time-frequency analysis of breathing dynamics are shown below. The respiratory frequency is bounded within the HF band (0.15-0.4 Hz) throughout whole experimental sessions including resting and emotional elicitation conditions, are shown in Fig 2. Therefore, it is possible to consider the HF power of HRV as a reliable marker of parasympathetic activity (2, 45, 50).

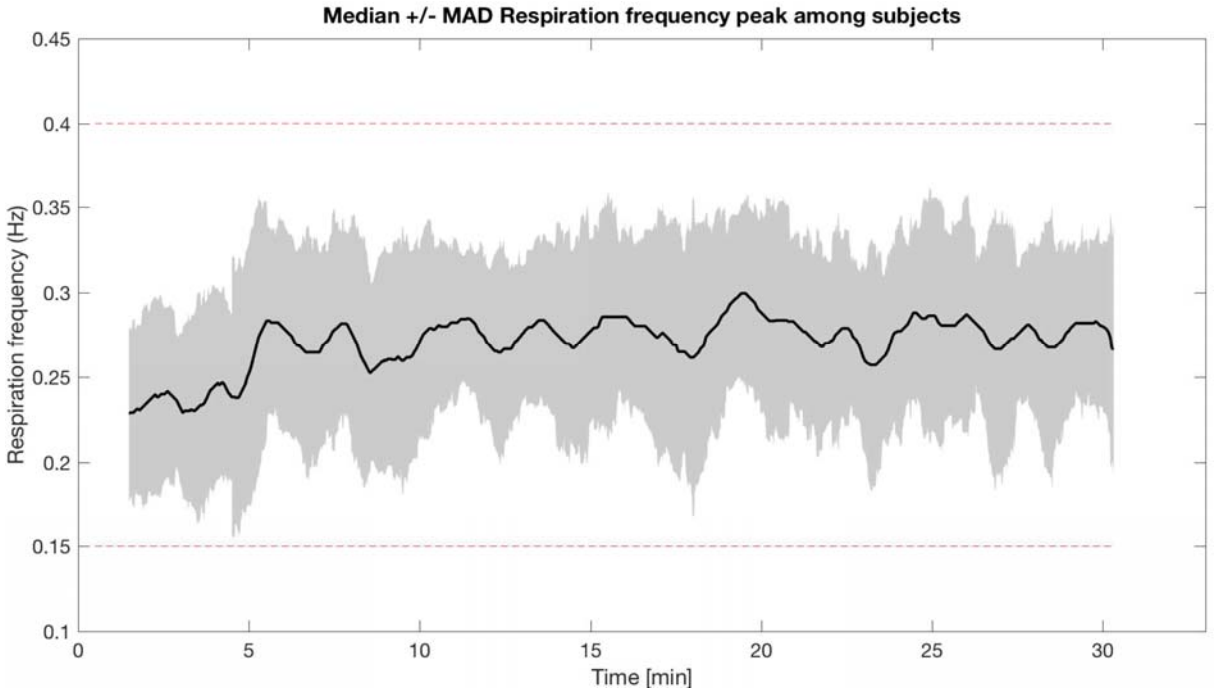

Fig. 2. Black lines and gray areas indicate median and MAD values among subjects of the smoothed respiratory time-frequency representation. Horizontal dashed lines mark the lower and upper bounds of the HRV-HF power spectrum.

III.A. Brain-to-heart directional coupling

Figure 1 and 2 show, for each experimental condition, topographic maps of the brain-to-heart GCI averaged across subjects (maps A-D), along with p-values resulting from the F-test (maps I-IV) and statistical comparison of GCI distributions between each pair of conditions (maps a-f). Considering the mean heartbeat dynamics as the cardiac process (Figure 1), therefore considering brain-to-heart dynamics through both sympathetic and parasympathetic nervous systems, a significant increase of the information transfer was found during emotional elicitation (Figure 1.B, 1.C, 1.D) with respect to the resting state (Figure1.A). Moreover, a valence-dependent lateralization effect of the information transfer can also be observed (Figure 1.b, 1.c). Particularly, the positive stimulation induces a significantly higher information transfer from the left-brain hemisphere to the heart, with a specific involvement of the somatosensory (as highlighted by the circle in the Figure 1.D), parietal, occipital, and prefrontal cortices. On the other hand, negative stimuli induce higher information transfer from the prefrontal and somatosensory right regions (as highlighted by the circle in the Figure 1.C), whereas in the parietal and occipital areas the GCI increases in both the left and right hemisphere.

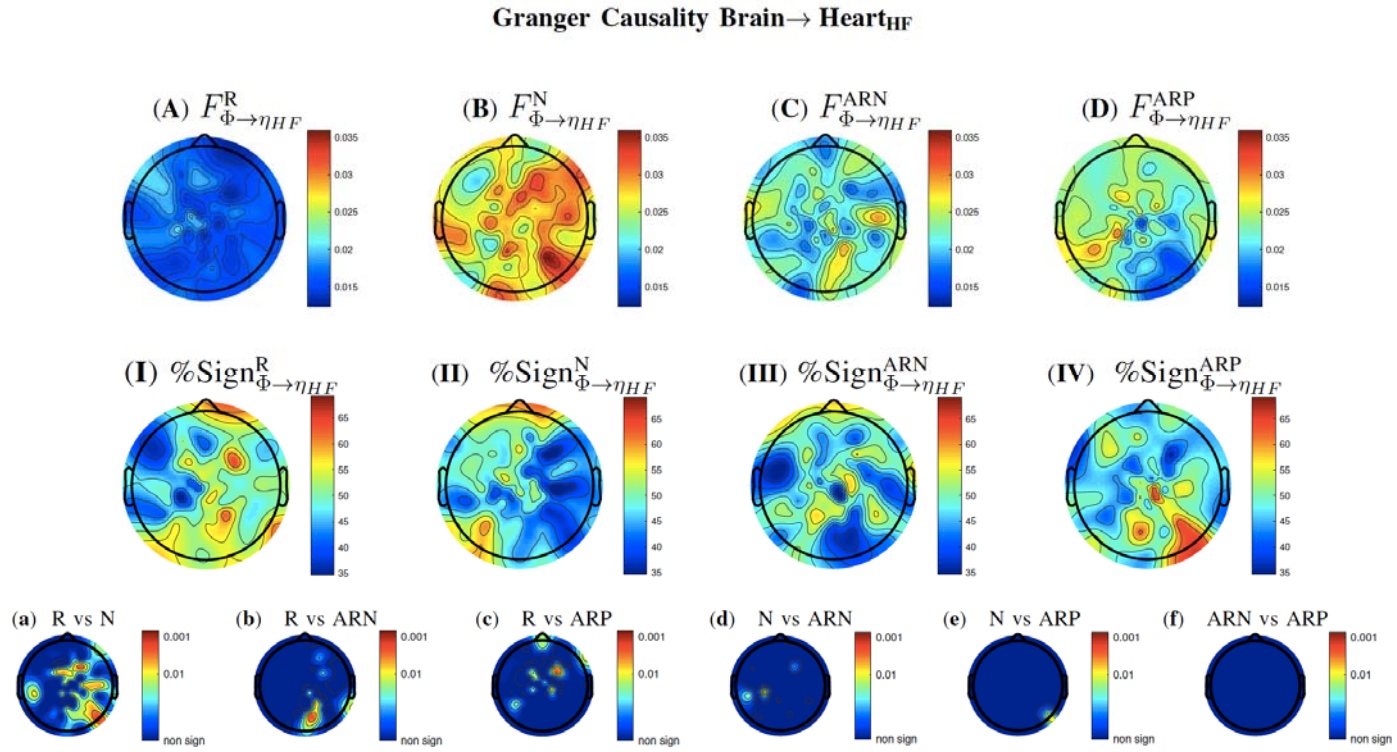

Fig. 3. Topographic maps in the first-row panel show Granger Causality values from EEG power spectrum computed in all frequency band to HRV power spectrum computed in HF band ($F_{\Phi\to\eta_{HF}}$). The four maps correspond to the four experimental conditions (R: rest; N: Neutral elicitation; ARN: Arousing elicitation with negative valence; ARP: Arousing elicitation with positive valence). In the second row, topographic maps represent percentage of subjects showing a significant GCI according to the F-test results for each electrode and experimental condition. In the third row, topographic maps give a graphical representation of post-hoc statistical results. The six maps correspond to the six pairwise comparisons among the four experimental conditions. Color scale shows p-values corrected for multiple comparisons.

Although only around 33% of subjects shows significant GCI these hemisphere-specific GCI increases are statistically significant with respect to the resting state, as shown by the p-values topographic maps comparing R sessions with ARP and ARN sessions. Moreover, the chi-squared test between the proportions of significant electrodes in the right and left hemisphere, confirms the evidence of the lateralization effect already observed through visual inspection. In fact, the proportion of significant areas in the left hemisphere was significantly higher than those in the right one, when comparing "R vs ARP" sessions, with a p-value of $8.96 \cdot 10^{-10}$ as seen in Table I.

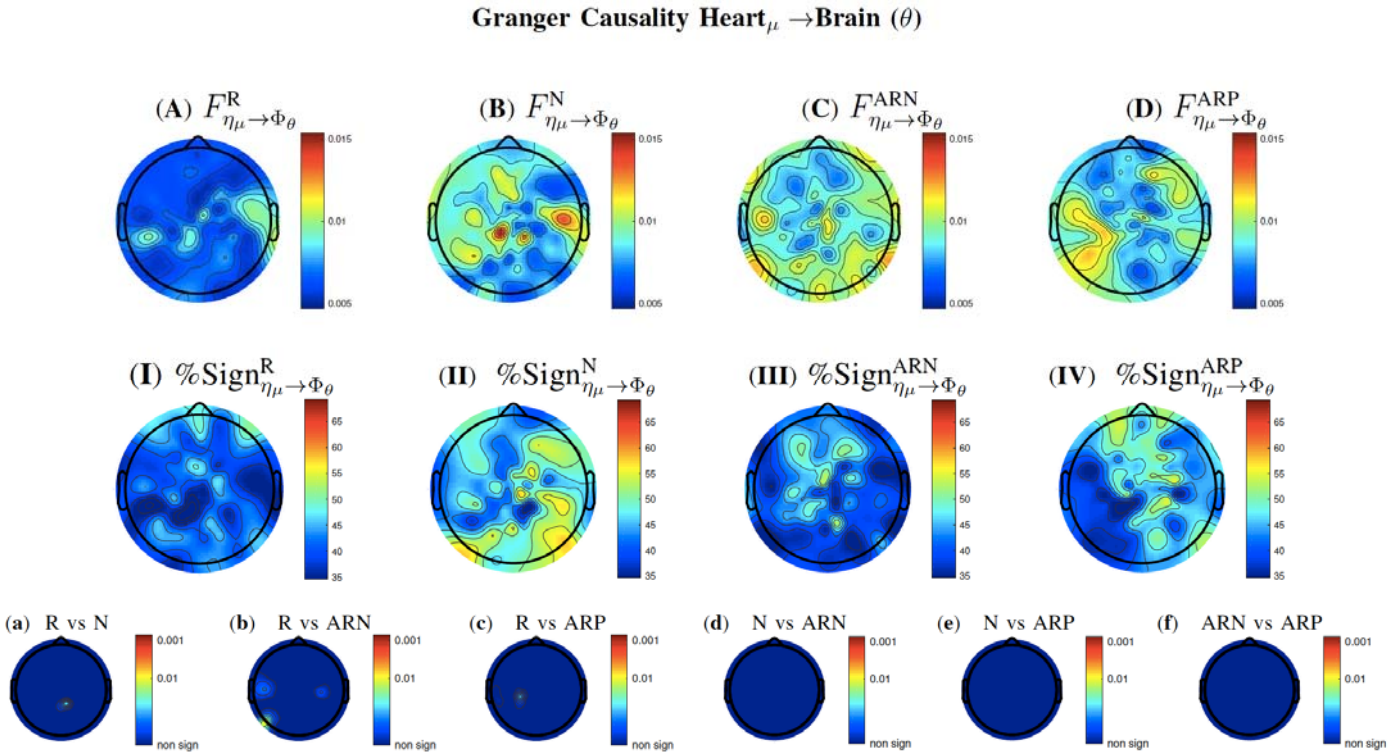

Fig. 4. Topographic maps in the first-row panel show Granger Causality values from instantaneous heart rate to EEG power spectrum computed in θ band ($F_{\eta \to \theta}$). The four maps correspond to the four experimental conditions (R: rest; N: Neutral elicitation; ARN: Arousing elicitation with negative valence; ARP: Arousing elicitation with positive valence). In the second row, topographic maps represent percentage of subjects showing a significant GCI according to the F-test results for each electrode and experimental condition. In the third row, topographic maps give a graphical representation of post-hoc statistical results. The six maps correspond to the six pairwise comparisons among the four experimental conditions. Color scale shows p-values corrected for multiple comparisons.

Considering the HF power dynamics as the cardiac process (Figure 2), therefore considering from-brain-to-heart dynamics through parasympathetic nervous system exclusively, a significant increase in GCI during neutral and arousing stimuli (Figure 2.B, 2.C, 2.D) with respect to the resting state (Figure 2.A) was found. GC analysis shows that a neutral visual stimulation induces a significant information transfer from the right hemisphere to the parasympathetic system (Figure 2.a), whereas the information transfer for positive (negative) stimuli originates from the frontal and prefrontal mid-line (right-posterior) areas (see Figure 2.a, and 2.b). Results from the F-tests indicate significant GCIs in over 50% of the subjects (up to 70%) in the majority of brain regions (Figure 2.I–2.IV). Furthermore, the significant increase of GCI in the right hemisphere, during negative and neutral elicitation with respect to the rest, is statistically higher than in the left one, as shown by the chi-squared test concerning the comparisons between “R vs ARN” and “R vs N” (see Table I).

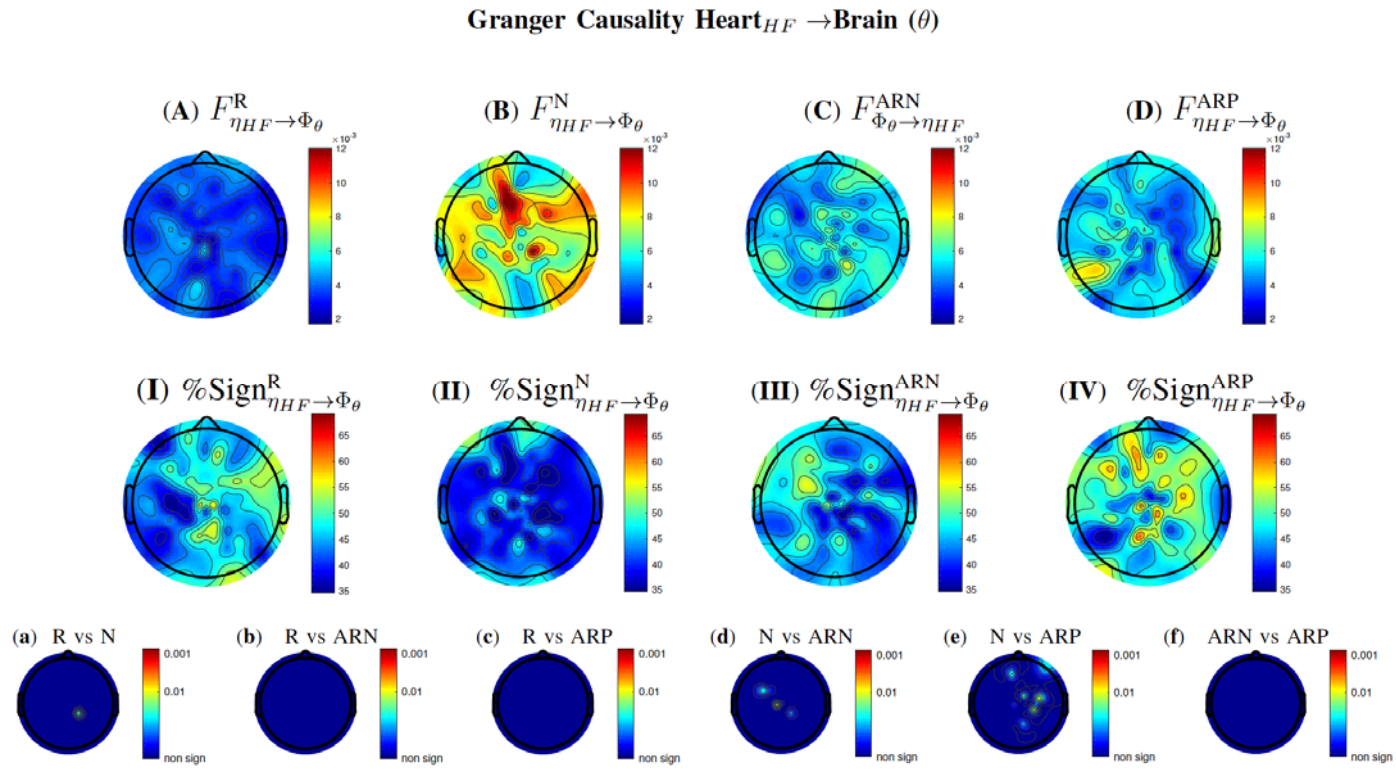

Fig. 5. Topographic maps in the first-row panel show Granger Causality values from HRV power spectrum computed in HF band to EEG power spectrum computed in θ band ($F_{HF\to\theta}$). The four maps correspond to the four experimental conditions (R: rest; N: Neutral elicitation; ARN: Arousing elicitation with negative valence; ARP: Arousing elicitation with positive valence). In the second row, topographic maps represent percentage of subjects showing a significant GCI according to the F-test results for each electrode and experimental condition. In the third row, topographic maps give a graphical representation of post-hoc statistical results. The six maps correspond to the six pairwise comparisons among the four experimental conditions. Color scale shows p-values corrected for multiple comparisons.

TABLE I

P-VALUES FROM CHI-SQUARED STATISTICS TO TEST THE SIGNIFICANCE OF THE DIFFERENCES BETWEEN THE TWO HEMISPHERES FOR EACH BRAIN-TO-HEART COMPARISON

Brain-to-Heart	R vs N	R vs ARN	R vs ARP	N vs ARN	N vs ARP	ARN vs ARP
$\Phi \to \eta_\mu$	0.637	0.174	**8.96e-10**	1.000	1.000	0.986
$\Phi \to \eta_{HF}$	**1.00e-15**	**1.06e-04**	0.758	0.979	0.314	1.000

III.B. Heart-to-Brain directional coupling

Considering the afferent coupling from heart to brain, Figures 3-10 show, for each experimental condition, topographic maps of GCI values averaged among all subjects (maps A-D), and p-value topographic maps resulting from the F-test (maps I-IV) and the multiple statistical comparisons between each pair of the four experimental conditions (maps a-f). Specifically, Figures 3-9 refer to the $\eta_\mu \to \Phi_{\theta,\alpha,\beta,\gamma}$ transfer, whereas Figures 4-10 to $\eta_{HF} \to \Phi_{\theta,\alpha,\beta,\gamma}$ transfer.

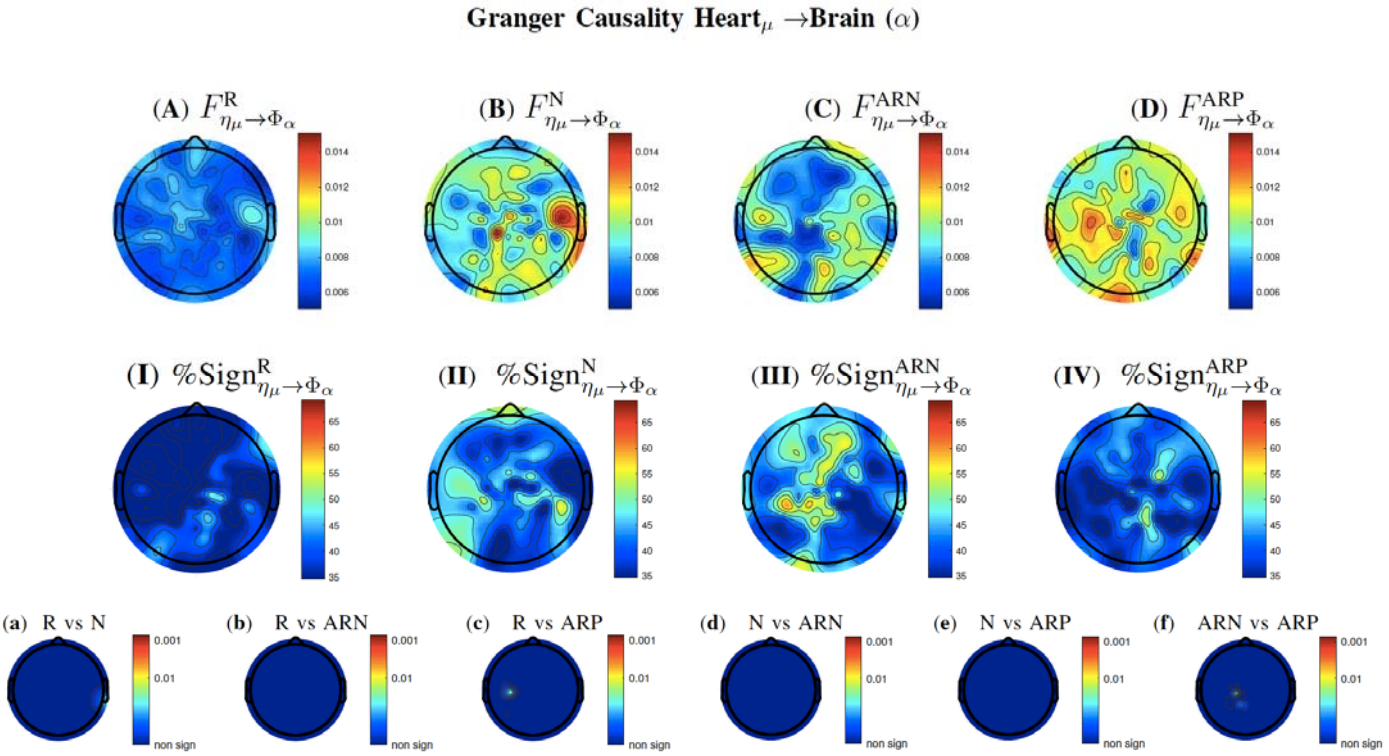

Fig. 6. Topographic maps in the first-row panel show Granger Causality values from instantaneous heart rate to EEG power spectrum computed in α band ($F_{\eta \to \alpha}$). The four maps correspond to the four experimental conditions (R: rest; N: Neutral elicitation; ARN: Arousing elicitation with negative valence; ARP: Arousing elicitation with positive valence). In the second row, topographic maps represent percentage of subjects showing a significant GCI according to the F-test results for each electrode and experimental condition. In the third row, topographic maps give a graphical representation of post-hoc statistical results. The six maps correspond to the six pairwise comparisons among the four experimental conditions. Color scale shows p-values corrected for multiple comparisons.

Considering the mean heartbeat dynamics and the EEG lowest frequency bands (i.e., θ and α) no significant variations among arousal, neutral, and resting sessions are found in the afferent transfer (Figure 3 Figure 5). However, taking into account brain oscillations in the β band (Figure 7), a lateralization effect of the information transfer during the positive emotional elicitation with respect to the resting state is evident in the left frontal and somatosensory areas (see Figure 7.c). This is also supported by the statistical results of the chi-squared test in Table II, which shows a significant variation between the two hemispheres in the R vs ARP comparison. In the γ band (Figure 9), similarly to the brain-to-heart analysis, we found a valence-dependent lateralization of information transfer, even though in a less marked way, as shown by p-value topographic maps related to the "R vs. ARN", and "R vs. ARP" comparisons (Figure 9.b and 9.c, respectively). In fact, statistical results (Table II) suggest that, comparing with resting state sessions, sympathetic and parasympathetic driven information is transferred prevalently to the left hemisphere cortex in case of positive arousing elicitation (Figure 9.c, and to the right hemisphere cortex in case of negative arousing elicitation (Figure 9.b). In addition, note that in the $F^{ARP}_{\Phi_\gamma \to \eta_\mu}$case, the percentage of subjects showing a significant GCI

(F-statistics <.05) during the positive elicitation was constantly over 50% (see Figure 9.IV).

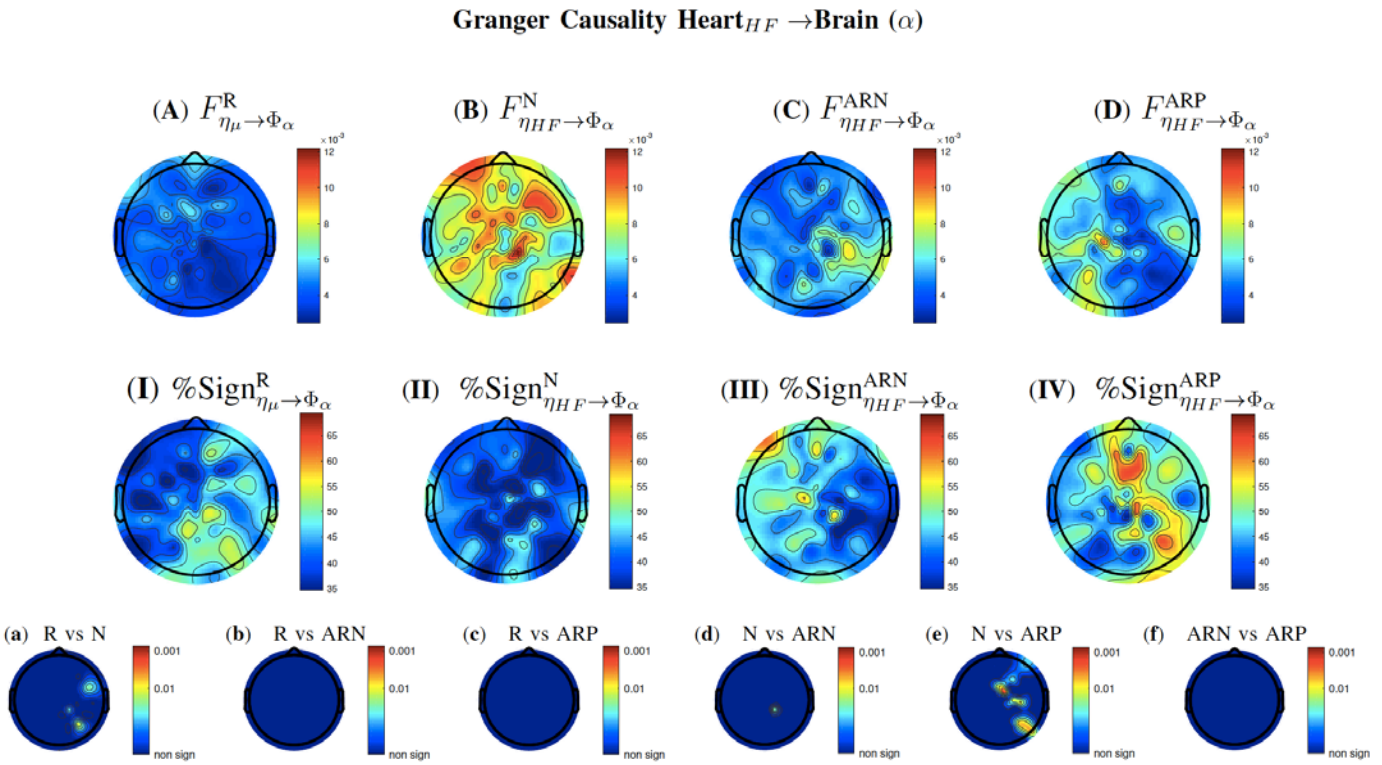

Fig. 7. Topographic maps in the first-row panel show Granger Causality values from HRV power spectrum computed in HF band to EEG power spectrum computed in α band ($F_{\eta \to \alpha}$). The four maps correspond to the four experimental conditions (R: rest; N: Neutral elicitation; ARN: Arousing elicitation with negative valence; ARP: Arousing elicitation with positive valence). In the second row, topographic maps represent percentage of subjects showing a significant GCI according to the F-test results for each electrode and experimental condition. In the third row, topographic maps give a graphical representation of post-hoc statistical results. The six maps correspond to the six pairwise comparisons among the four experimental conditions. Color scale shows p-values corrected for multiple comparisons.

Concerning the parasympathetic-driven information transfer to the brain, significant changes are associated with neutral vs. positive visual elicitation (Figure 4 and 6). Specifically, in the θ and α bands, comparing positive and neutral stimuli, a significant decrease of the GC values computed in the right hemisphere was found during the positive stimuli with respect to the neutral stimuli (see Figure 4.e and 6.e, respectively). Moreover, considering the α band, the "N vs ARP" comparison revealed also a significant difference between the two hemispheres as see in Table II. This lateralization effect related to the positive stimulation in the right hemisphere is lost in the β (Figure 8) and γ bands (Figure 10), although in the latter band there is a significant decrease of the information transfer between vagal dynamics and the brain involving the parietal cortices area (Figure 10.e).

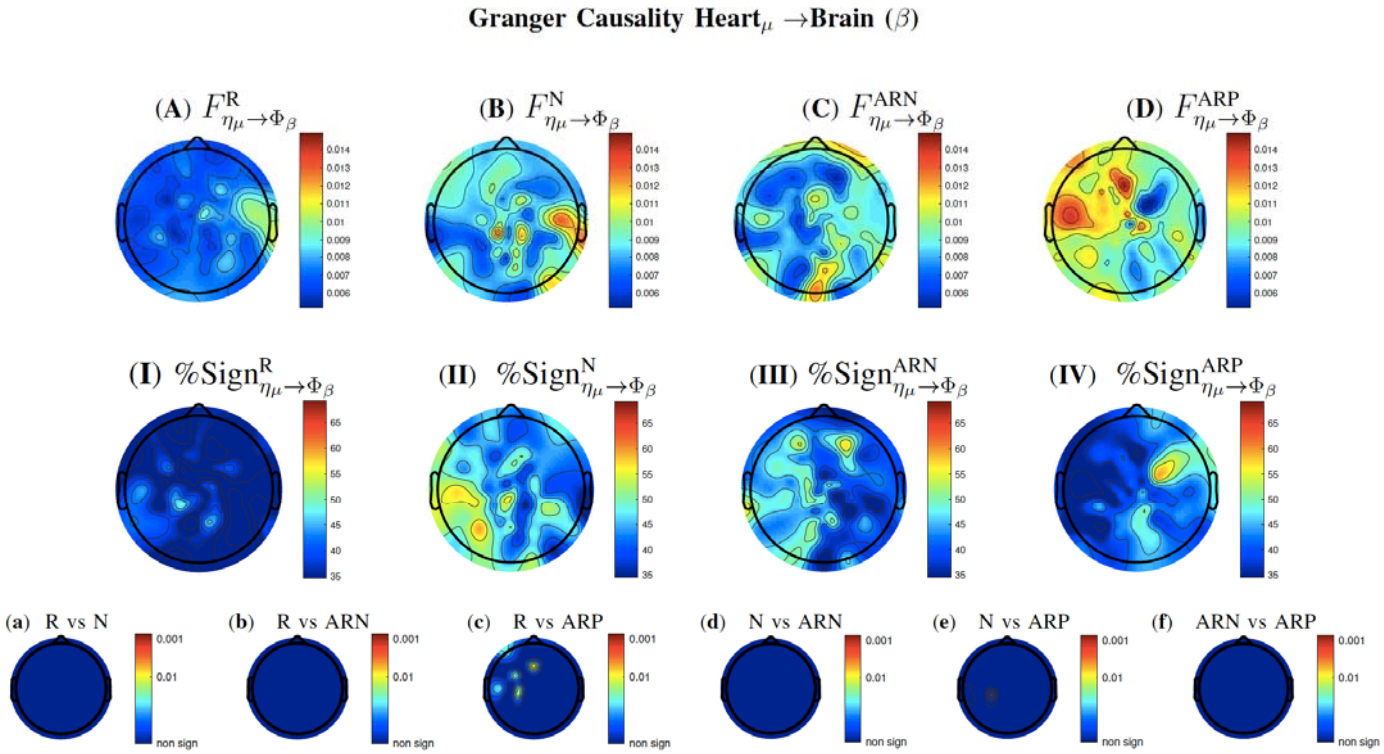

Fig. 8. Topographic maps in the first-row panel show Granger Causality values from instantaneous heart rate to EEG power spectrum computed in β band ($F_{\eta\to\beta}$). The four maps correspond to the four experimental conditions (R: rest; N: Neutral elicitation; ARN: Arousing elicitation with negative valence; ARP: Arousing elicitation with positive valence). In the second row, topographic maps represent percentage of subjects showing a significant GCI according to the F-test results for each electrode and experimental condition. In the third row, topographic maps give a graphical representation of post-hoc statistical results. The six maps correspond to the six pairwise comparisons among the four experimental conditions. Color scale shows p-values corrected for multiple comparisons.

IV. Discussion and Conclusion

The aim of this study was to assess functional, directional brain-heart interactions during visual emotional elicitation in healthy subjects. Specifically, the instantaneous mean RR interval (μ) and the instantaneous HF power estimated from a point-process modeling are taken as realizations of heartbeat dynamics, whereas brain dynamics are estimated through EEG power spectra. The use of HRV as a gold-standard sign of ANS control is especially justified for the present study by its extensive use and effectiveness in previous research in affective computing (see (11, 16, 33, 38, 58) and references therein for reviews). Likewise, EEG and evoked related potentials recordings have been extensively employed to investigate brain dynamics during emotional processing and regulation (11, 48, 65), with a particular focus on the so-called brain asymmetry and the lateralization theory during emotional processing (9, 20, 52).

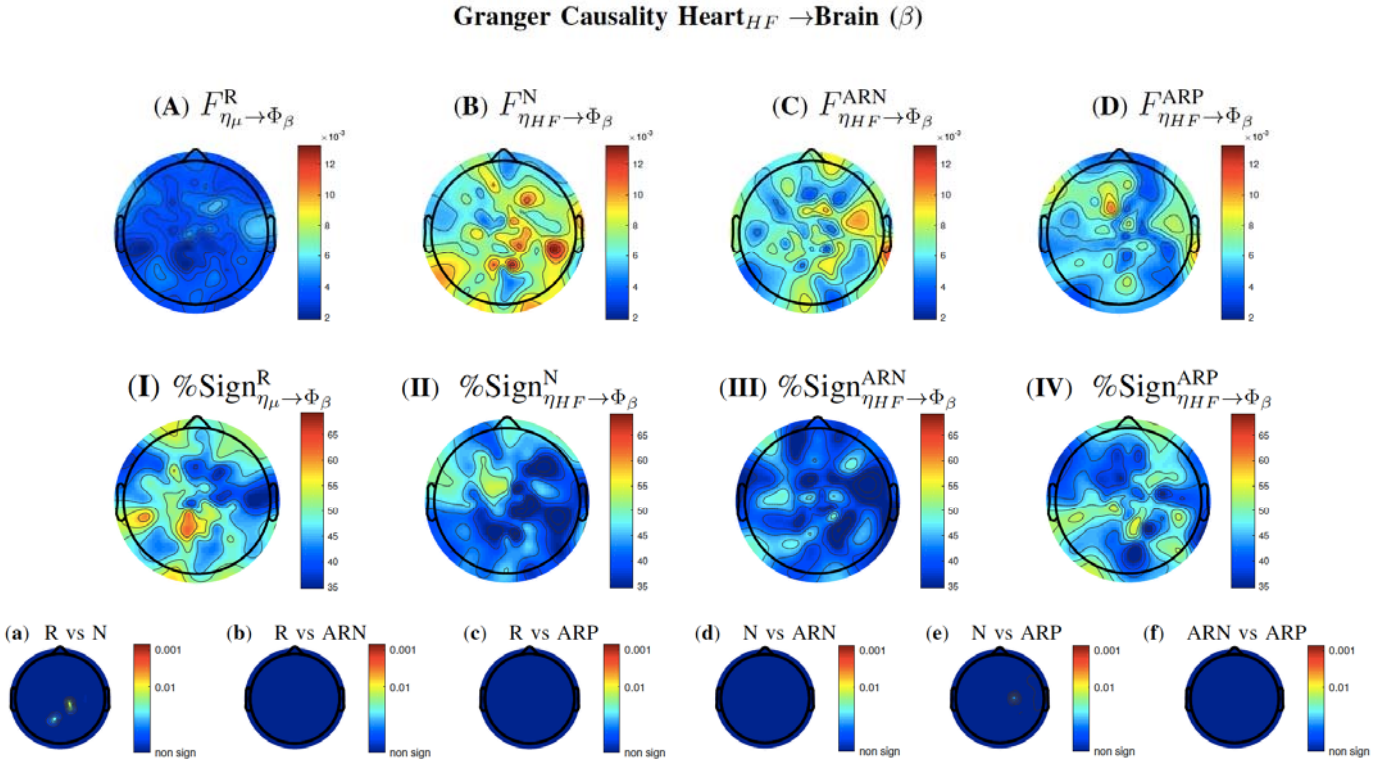

Fig. 9. Topographic maps in the first-row panel show Granger Causality values from HRV power spectrum computed in HF band to EEG power spectrum computed in β band ($F_{\eta \to \beta}$). The four maps correspond to the four experimental conditions (R: rest; N: Neutral elicitation; ARN: Arousing elicitation with negative valence; ARP: Arousing elicitation with positive valence). In the second row, topographic maps represent percentage of subjects showing a significant GCI according to the F-test results for each electrode and experimental condition. In the third row, topographic maps give a graphical representation of post-hoc statistical results. The six maps correspond to the six pairwise comparisons among the four experimental conditions. Color scale shows p-values corrected for multiple comparisons.

TABLE II

P-VALUES FROM CHI-SQUARED STATISTICS TO TEST THE SIGNIFICANCE OF THE DIFFERENCES BETWEEN THE TWO HEMISPHERES FOR EACH HEART-TO-BRAIN COMPARISON

Heart-to-Brain	R vs N	R vs ARN	R vs ARP	N vs ARN	N vs ARP	ARN vs ARP
$\eta_\mu \to \Phi_\theta$	0.314	0.526	0.302	1	1	1
$\eta_\mu \to \Phi_\alpha$	0.302	1	0.314	1	1	0.063
$\eta_\mu \to \Phi_\beta$	1	1	**0.012**	1	0.302	1
$\eta_\mu \to \Phi_\gamma$	0.302	**0.032**	0.061	0.314	1	1
$\eta_{HF} \to \Phi_\theta$	0.314	1	1	0.268	0.205	1
$\eta_{HF} \to \Phi_\alpha$	0.07	1	1	0.314	**3.15E-04**	1
$\eta_{HF} \to \Phi_\beta$	0.556	1	1	1	0.314	1
$\eta_{HF} \to \Phi_\gamma$	0.314	1	0.314	1	0.105	1

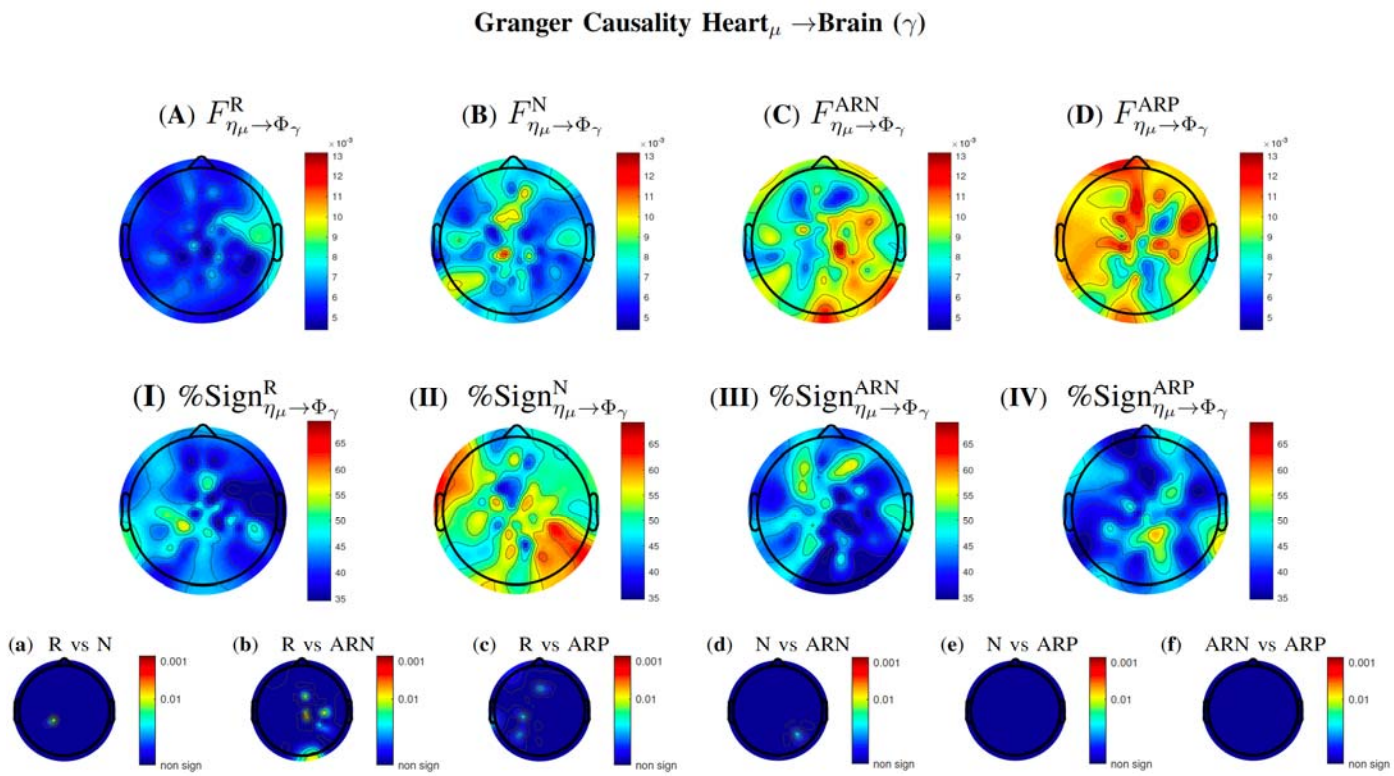

Fig. 10. Topographic maps in the first-row panel show Granger Causality values from instantaneous heart rate to EEG power spectrum computed in γ band ($F_{\eta\to\gamma}$). The four maps correspond to the four experimental conditions (R: rest; N: Neutral elicitation; ARN: Arousing elicitation with negative valence; ARP: Arousing elicitation with positive valence). In the second row, topographic maps represent percentage of subjects showing a significant GCI according to the F-test results for each electrode and experimental condition. In the third row, topographic maps give a graphical representation of post-hoc statistical results. The six maps correspond to the six pairwise comparisons among the four experimental conditions. Color scale shows p-values corrected for multiple comparisons.

To the best of our knowledge, this is the first study that investigates the dynamic causal interactions between the brain and heart and attempts to estimate their coupling using a directional multivariate model to understand emotional regulation processes. We focused on GC to properly measure interactions between time series of the EEG oscillatory activity and instantaneous heartbeat dynamics, also inferring on the functional causality from-brain-to-heart and from-heart-to-brain. Importantly, GC implements a statistical, predictive notion of causality whereby fluctuations in one system (e.g., the brain) precede and help predicting subsequent fluctuations in the second system (e.g., heart). As multivariate GC input setting, we considered high-resolution (i.e., 128 channels) EEG oscillations for each of the four canonical bands: θ (4-8 Hz), α (8-14 Hz), β (14-32 Hz), and γ (32-45 Hz), as well as instantaneous heartbeat and vagal estimates from point-process models. The latter choice is justified by three main observations: i) this modeling has been successfully applied for effective emotion recognition (76); ii) it is possible to obtain cardiovascular estimates of sympathovagal tone with any resolution in time, without the need for preliminary

interpolation of the unevenly sampled RR interval series (76); iii) proper model goodness of fit measures can be studied to demonstrate that the derived estimates actually fit the individual cardiac series (76).

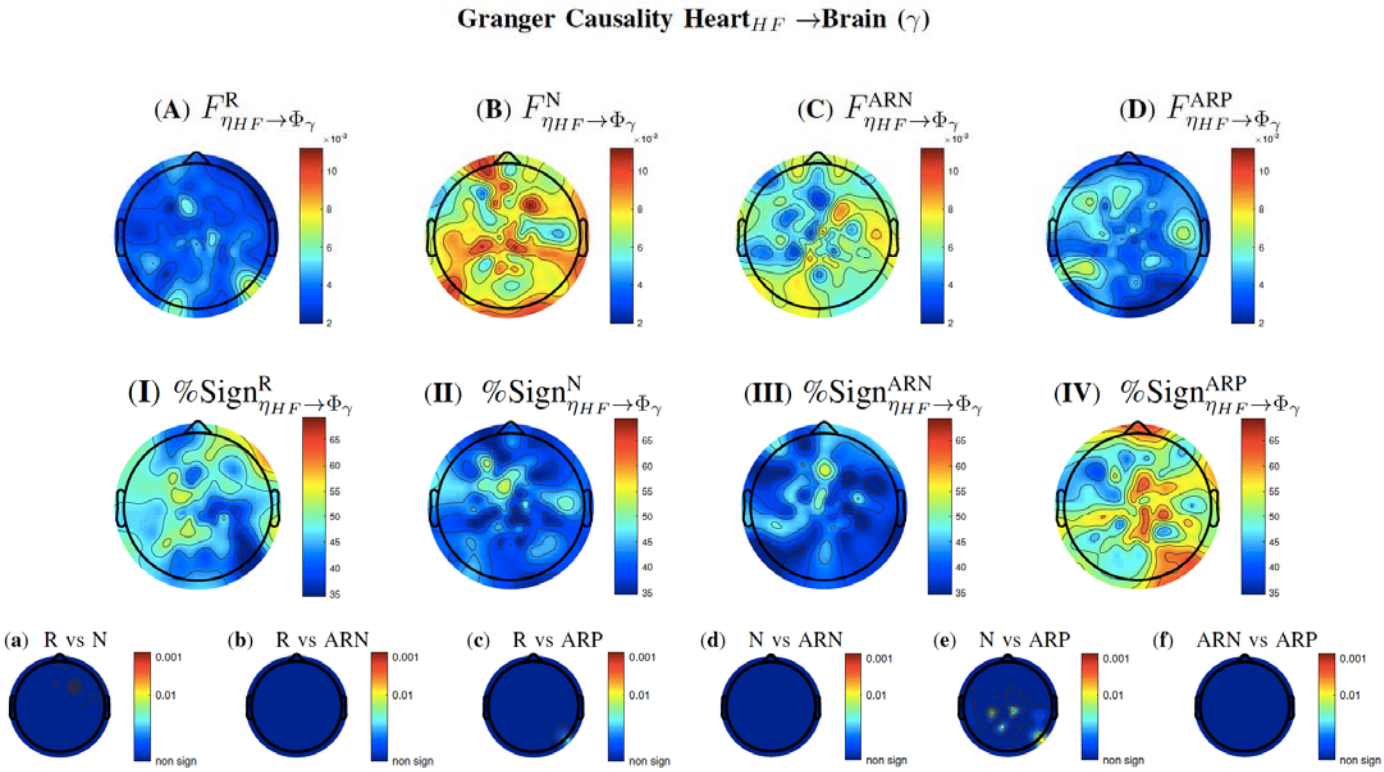

Fig. 11. Topographic maps in the first-row panel show Granger Causality values from HRV power spectrum computed in HF band to EEG power spectrum computed in γ band ($F_{\eta\to\gamma}$). The four maps correspond to the four experimental conditions (R: rest; N: Neutral elicitation; ARN: Arousing elicitation with negative valence; ARP: Arousing elicitation with positive valence). In the second row, topographic maps represent percentage of subjects showing a significant GCI according to the F-test results for each electrode and experimental condition. In the third row, topographic maps give a graphical representation of post-hoc statistical results. The six maps correspond to the six pairwise comparisons among the four experimental conditions. Color scale shows p-values corrected for multiple comparisons.

Twenty-two healthy subjects were shown standardized affective pictures taken from the IAPS database. We selected five different groups of images according to their arousal levels (N, AR1, AR2, AR3, AR4). Each group is comprised of two different valence levels. Note that in the proposed methodological approach not only we consider all possible valence-dependent brain-heart couplings regardless of the arousal level, but also account for the subject-specific time-varying coupling in a directional fashion. In addition, we estimated the parasympathetic nervous system dynamics through the instantaneous HF power spectrum derived from the point-process model. This allowed us to study the dynamics of the causal information transfer between the central neural activity and the parasympathetic system during emotional elicitation.

Our findings demonstrate that the functional causal coupling between brain and heartbeat dynamics during emotional elicitation is characterized by a significant valence-dependent lateralization with respect to resting states. Specifically, during a

positive visual elicitation information is transferred from the left-brain hemisphere to the heart, whereas during negative elicitation GC increases in the right prefrontal region. The valence-dependent lateralization is also evident considering the from-heart-to-brain path probed for high/frequency EEG rhythms (i.e., β and γ bands). In fact, positive elicitations determine an increased transfer of information from the heart to the left-frontal and somatosensory regions. In addition, considering EEG oscillations in the γ band, the information transfer between rest and negative elicitation is directed toward the somatosensory and occipital right cortices. Moreover, according to the F-test performed for all the $brain_{\Phi}$-$heart_{\eta}$/ $heart_{\eta}$-$brain_{\Phi}$ GC values, the predictive information is statistically significant in up to 70% of the subjects. This demonstrates a large inter-subject variability that commonly characterizes physiological responses to emotional elicitation. However, it is worthwhile noting that the brain regions where the statistical comparison between R, N, ARN, and ARP is statistically significant also show a high percentage of subjects with significant GCI ($\geq 50\%$ (24)).

Of note, the current literature reports controversial theories and experimental results on lateralization as correlated with the perception of emotional valence. There is a substantial body of work claiming evidence of an overall right-lateralization of emotional processing, subsumed by the so-called *Right-Hemisphere* model (1, 9, 60, 63). Although evidences for the right-hemisphere hypothesis are numerous, many studies describe hemispheric differences as a function of positive versus negative emotions (22, 68, 82). As a matter of fact, there are evidences supporting the hypothesis of an increased EEG activity over the left hemisphere associated with positive affective processing as compared to the right hemisphere, which is, instead, thought to be involved in negative emotional processing (67, 74). Conversely, other findings show relatively higher power for negative valence over the left temporal region as compared to the right and a general lateralization shift towards the right hemisphere for positive valence (51).

There is ample evidence that efferent innervation of the heart is lateralized in the peripheral part of the autonomic system with right-sided and left-sided autonomic pathways influencing cardiac activity in an asymmetric manner (43, 62, 69, 70). The SA node is predominantly and more efficiently controlled by sympathetic and parasympathetic fibers running on the right side. Considering this lateralization of autonomic cardiac control at the peripheral level, and since most of the autonomic pathways descending from brain stem areas take an ipsilateral route, several studies have suggested an analogous mode or organization at the level of the central nervous system (30, 40, 49). Indeed, it is not surprising to find that brain stem regions immediately involved in autonomic regulation of cardiac activity, such as hypothalamic or medullary areas, seem to be lateralized in the same manner as the peripheral pathways. On the other side, also in this case the scientific literature is not always coherent. Other findings indicate indeed that the control of autonomic cardiac activity at the level of the cerebral cortex seems to be characterized by a division of responsibility between both hemispheres, i.e., sympathetic activity is mainly controlled by the

right hemisphere and parasympathetic activity is under the left hemisphere's main control (83).

Here, we report that visual emotional stimulation determines a transfer of information from the right brain hemisphere to vagal nerve related activity when the stimulation is neutral, and from the posterior right area when the stimulation is unpleasant. On the contrary, during positive elicitation the action of the medial prefrontal and frontal cortex prevails. The lateralization effect is more evident in the afferent connection from the parasympathetic system to the brain. The comparison between a positive arousing state with a neutral one where the parasympathetic tone is dominant shows a significant increase in the right hemisphere in this latter condition. Therefore, we confirm the relevance of the right hemisphere in the sympathovagal activity, but we also highlight the importance of the hedonic tract of the emotional elicitation. Of note, our considerations were not limited to visual inspection but were supported by the chi-squared test, which statistically evaluates the differences between the two hemispheres. Our findings support the so-called *Dual-System Models* of emotions (52). Contrary to the *Right-Hemisphere* hypothesis that states a dominant role for the right hemisphere in emotional processing (1, 8, 9, 60), Dual-System theories suggest that positive and negative emotions are implemented by neural systems that are at least partially separable (20, 36, 59). Indeed, although in the current literature there are several different theories, perhaps one of the most influential is the valence asymmetry model (20).

As a study limitation, we mention that data from valence elicitation sessions comprised stimuli across different degrees of arousal (from 1 to 10, according to IAPS scale (78)); as a consequence, the reported results "mix" different arousing levels administrated with constant valence, and, therefore, might be obtained through non-optimal VAR model parameter estimation because of possible non-stationarities of the input data. Moreover, we mention that self-assessment scores of elicited IAPS images after the experiment were not taken into account in this study. We rely, in fact, on the standardization of the IAPS images, which is performed on a very large number of healthy subjects (42), ensuring highly consistent results in terms of valence and arousal ratings. Moreover, it is worthwhile noting that GC may not underlie anatomical connections between cardiovascular system and brain, but it measures the ability to predict the future values of a time series using prior values of another. What can be measured (and what cannot) by statistical measures such as Granger causality has been matter of intense debate in the recent literature (see, e.g., (5, 28, 34, 66)). As pointed in a recent discussion (5), the design and purpose of GC is to measure "the effect" that physical mechanisms (i.e., physiological mechanisms) have on the time series which are measured as output of two observed dynamical systems (in our case, organ systems). Through its underlying statistical notion (i.e., quantifying the reduction in the prediction error when the causal mechanism is taken into account, as compared to when it is ignored), GC quantifies the directed influence (or "causal information transfer") from one system to another intended purely from a statistical, data-driven perspective. As such, GC measures of the causal effect produced by an underlying mechanism

yield estimates of the "functional connectivity" between systems, as opposed to physiology-driven parametric models such as dynamic causal modeling which attempt to find the optimal mechanistic description explaining the observed data in terms of "effective connectivity" (66). It is worth noting that neither "functional" nor "effective" connectivity representations necessarily map univocally onto the underlying anatomical (structural) connectivity. Therefore, GC is necessarily limited if one tries to elicit the exact specific (afferent or efferent) physiological mechanisms which give rise to an observed phenomenon (like an emotion in our case). Nevertheless, if properly computed from multivariate linear processes, GC is a clear and unambiguous measure of causal effect, and can thus be interpreted to detect correlated dynamics between two systems (here, brain and cardiovascular system) where temporal precedence serves to disambiguate cause and effect (here, to set directed statistical influences between central neural effects manifested in the EEG rhythms and "peripheral" effects manifested in the ANS dynamic control of heart rate).

As part of our inference is related to the quantification of functional brain-heart coupling through vagal dynamics, we demonstrated that the respiratory frequency is bounded within the HF band (0.14-0.40 Hz) throughout the emotional elicitation. Moreover, no significant changes in such a breathing frequency were observed between sessions. Therefore, it is possible to conclude that our estimate of HF power is indeed a reliable marker of parasympathetic activity (2), being related to respiration dynamics through the phenomenon of respiratory sinus arrhythmia (2, 45, 50). Moreover, since breathing is under direct cortical control (44), the variability observed in the EEG series may be modulated by cardio-respiratory changes that contribute to brain-heart interactions. Thus, respiratory activity is likely to be one of the physiological factors explaining the altered information transfer between heart and brain dynamics that we have observed during a visual emotional processing. From this viewpoint, our estimates of causal brain-heart interplay during emotional elicitation should be interpreted as a quantification of the functional coupling between parasympathetic and cortical dynamics, which might be primarily influenced by breathing. Other influences from hormonal and, in general, biological variables involved in the complex process of bodily regulation of emotional arousal cannot be excluded as well.

Furthermore, at a speculation level, our results suggest that emotional processing is mainly linked to a bidirectional information transfer between the heart and brain areas belonging to the so-called central autonomic network (CAN (6, 13, 61, 81), which includes brainstem nuclei, and a number of forebrain regions including the cingulate cortex, insula, medial prefrontal cortex, thalamus, amygdala, and hypothalamus (see (7) for details). However, since our study concerns cortical dynamics estimated through EEG, it is not possible to speculate on the specific CAN sub-regions activity involved in the brain-heart communication during emotional experience. As the sympathetic and parasympathetic autonomic branches interact at the level of the atrial sinus node to concurrently regulate heart rate and, consequently, blood pressure and respiration dynamics (6,13), we

hypothesize that from-heart-to-brain information transfer results from a multivariate, complex interaction between baroreflex-mediated cardio-respiratory nonlinear dynamics.

V. PERSPECTIVES

Findings of this study pave the path towards the understanding of the so-called "origin" of emotions as well as the neurophysiological path of emotional processing, which are being debated from the methodological and neuroscientific viewpoints. The proposed approach may be adapted to process neuroimaging data collected along with ANS markers, maybe extending the methodological estimates to the complex/nonlinear domain of heartbeat dynamics. Given the peculiar role of vagal and cortical dynamics in attentional significance of emotions (3, 17, 19, 32, 78), further investigations may include other measures of information storage (e.g., self-entropy) (26). Furthermore, these findings may constitute a reference evidence for the understanding of physio-pathological mechanisms in case of psychiatric/mental disorders, including e.g. depression and bipolar disorder.

VI. GRANTS

This study has received partial funding from the European Union's Horizon 2020 research and innovation program under the grant agreement No 824153 "Promoting social interaction through emotional body odours" - "POTION".

VII. DISCOLOSURES

None of the authors has any conflict of interest.

.

References

[1] Adolphs, R., Damasio, H., Tranel, D., and Damasio, A. R. (1996). Cortical systems for the recognition of emotion in facial expressions. Journal of neuroscience, 16(23):7678–7687.

[2] Akselrod, S., Gordon, D., Ubel, F. A., Shannon, D. C., Berger, A. C., \& Cohen, R. J. (1981). Power spectrum analysis of heart rate fluctuation: a quantitative probe of beat-to-beat cardiovascular control. science, 213(4504), 220-222.

[3] Balconi, M., Brambilla, E., and Falbo, L. (2009). Bis/bas, cortical oscillations and coherence in response to emotional cues. Brain research bulletin, 80(3):151–157.

[4] Barnett, L. and Seth, A. K. (2015). Granger causality for state-space models. Phys. Rev. E, 91(4):040101.

[5] Barrett, A. B. and Barnett, L. (2013). Granger causality is designed to measure effect, not mechanism. Frontiers in neuroinformatics, 7:6.

[6] Benarroch, E. E. (1993). The central autonomic network: functional organization, dysfunction, and perspective. In Mayo Clinic Proceedings, volume 68, pages 988–1001. Elsevier

[7] Benarroch, E. E. (2012). Central autonomic control. In Primer on the Autonomic Nervous System (Third Edition), pages 9–12. Elsevier.

[8] Borod, J. (2001). Asymmetries of emotional perception and expression in normal adults. Handbook of neuropsychology.

[9] Borod, J. C., Cicero, B. A., Obler, L. K., Welkowitz, J., Erhan, H. M., Santschi, C., Grunwald, I. S., Agosti, R. M., and Whalen, J. R. (1998). Right hemisphere emotional perception: Evidence across multiple channels. NEUROPSYCHOLOGY-NEW YORK-, 12:446–458.

[10] Bressler, S. L. and Seth, A. K. (2011). Wiener–granger causality: a well-established methodology. Neuroimage, 58(2):323–329.

[11] Calvo, R., D'Mello, S., et al. (2010). Affect detection: An interdisciplinary review of models, methods, and their applications. Affective Computing, IEEE Transactions on, 1(1):18–37.

[12] Cameron, O. G. (2001). Visceral sensory neuroscience: interoception. Oxford University Press.

[13] Cechetto, D.F., S. C. (1990). Role of the cerebral cortex in autonomic function. Central regulation of autonomic functions, pages 208–223.

[14] Cerqueira, J. J., Mailliet, F., Almeida, O. F., Jay, T. M., and Sousa, N. (2007). The prefrontal cortex as a key target of the maladaptive response to stress. Journal of Neuroscience, 27(11):2781–2787.

[15] Christianson, S.-A. (2014). The handbook of emotion and memory: Research and theory. Psychology Press.

[16] Coan, J. A. and Allen, J. J. (2007). Handbook of emotion elicitation and assessment. Oxford university press.

[17] Craig, A. (2003). Pain mechanisms: labeled lines versus convergence in central processing. Annual review of neuroscience, 26(1):1–30.

[18] Critchley, H. D., Wiens, S., Rotshtein, P., O¨ hman, A., and Dolan, R. J. (2004). Neural systems supporting interoceptive awareness. Nature neuroscience, 7(2):189.

[19] Damasio, A. R. (1998). Emotion in the perspective of an integrated nervous system. Brain research reviews, 26(2):83–86.

[20] Davidson, R. J. (1984). 11 affect, cognition, and hemispheric specialization. Emotions, cognition, and behavior, page 320.

[21] Delorme, A. and Makeig, S. (2004). Eeglab: an open source toolbox for analysis of single-trial eeg dynamics including independent component analysis. Journal of neuroscience methods, 134(1):9–21.

[22] Demaree, H. A., Everhart, D. E., Youngstrom, E. A., and Harrison, D. W. (2005). Brain lateralization of emotional processing: historical roots and a future incorporating "dominance", Behavioral and cognitive neuroscience reviews, 4(1):3– 20.

[23] Faes, L., Greco, A., Lanata, A., Barbieri, R., Scilingo, E. P., and Valenza, G. (2017a). Causal brain-heart information transfer during visual emotional elicitation in healthy subjects: Preliminary evaluations and future perspectives. In Engineering in Medicine and Biology Society (EMBC), 2017 39th Annual International Conference of the IEEE, pages 1559–1562. IEEE.

[24] Faes, L., Nollo, G., Jurysta, F., and Marinazzo, D. (2014). Information dynamics of brain–heart physiological networks during sleep. New Journal of Physics, 16(10):105005.

[25] Faes, L., Nollo, G., Stramaglia, S., and Marinazzo, D. (2017b). Multiscale granger causality. Physical Review E, 96(4):042150.

[26] Faes, L., Porta, A., Nollo, G., and Javorka, M. (2017c). Information decomposition in multivariate systems: definitions, implementation and application to cardiovascular networks. Entropy, 19(1):5.

[27] Foreman, R. and Chandler, M. (1994). Vagal afferent modulation of cardiac pain. Vagal control of the heart: experimental basis and clinical implications. Armonk, New York: Futura Publishing Co, pages 345–368.

[28] Friston, K., Moran, R., and Seth, A. K. (2013). Analysing connectivity with granger causality and dynamic causal modelling. Current opinion in neurobiology, 23(2):172–178.

[29] Frysinger, R. C. and Harper, R. M. (1990). Cardiac and respiratory correlations with unit discharge in epileptic human temporal lobe. Epilepsia, 31(2):162–171.

[30] Gatti, P. J., Johnson, T. A., and Massari, V. J. (1996). Can neurons in the nucleus ambiguus selectively regulate cardiac rate and atrio-ventricular conduction? Journal of the autonomic nervous system, 57(1):123–127.

[31] Granger, C. W. (1969). Investigating causal relations by econometric models and cross-spectral methods. Econometrica:

Journal of the Econometric Society, pages 424–438.

[32] Hagemann, D., Waldstein, S. R., and Thayer, J. F. (2003). Central and autonomic nervous system integration in emotion. Brain and cognition, 52(1):79–87.

[33] Henry, B. L., Minassian, A., Paulus, M. P., Geyer, M. A., and Perry, W. (2010). Heart rate variability in bipolar mania and schizophrenia. Journal of psychiatric research, 44(3):168–176.

[34] Hu, S., Dai, G., Worrell, G. A., Dai, Q., and Liang, H. (2011). Causality analysis of neural connectivity: critical examination of existing methods and advances of new methods. IEEE transactions on neural networks, 22(6):829–844.

[35] Jung, T.-P., Makeig, S., Westerfield, M., Townsend, J., Courchesne, E., and Sejnowski, T. J. (2000). Removal of eye activity artifacts from visual event-related potentials in normal and clinical subjects. Clinical Neurophysiology, 111(10):1745–1758.

[36] Kalin, N. H., Larson, C., Shelton, S. E., and Davidson, R. J. (1998). Asymmetric frontal brain activity, cortisol, and behavior associated with fearful temperament in rhesus monkeys. Behavioral neuroscience, 112(2):286.

[37] Kober, H., Barrett, L. F., Joseph, J., Bliss-Moreau, E., Lindquist, K., and Wager, T. D. (2008). Functional grouping and cortical–subcortical interactions in emotion: a meta-analysis of neuroimaging studies. Neuroimage, 42(2):998–1031.

[38] Kreibig, S. D. (2010). Autonomic nervous system activity in emotion: A review. Biological psychology, 84(3):394–421.

[39] Kroenke, K., Spitzer, R. L., and Williams, J. B. (2001). The phq-9. Journal of general internal medicine, 16(9):606–613.

[40] Kuo, J., Chai, C., Lee, T., Liu, C., and Lim, R. (1970). Localization of central cardiovascular control mechanism in the brain stem of the monkey. Experimental neurology, 29(1):131–141.

[41] Lamm, C. and Singer, T. (2010). The role of anterior insular cortex in social emotions. Brain Structure and Function, 214(5-6):579–591.

[42] Lang, P. and Bradley, M. M. (2007). The international affective picture system (IAPS) in the study of emotion and attention. Handbook of emotion elicitation and assessment, 29.

[43] Levy, M. N. and Martin, P. J. (1984). Neural control of the heart. In Physiology and Pathophysiology of the Heart, pages 337–354. Springer.

[44] Macefield, G., \& Gandevia, S. C. (1991). The cortical drive to human respiratory muscles in the awake state assessed by premotor cerebral potentials. The Journal of Physiology, 439(1), 545-558.

[45] Malpas, S. C. (2002). Neural influences on cardiovascular variability: possibilities and pitfalls. American Journal of Physiology-Heart and Circulatory Physiology, 282(1), H6-H20.

[46] Makovac, E., Garfinkel, S. N., Bassi, A., Basile, B., Macaluso, E., Cercignani, M., Calcagnini, G., Mattei, E., Agalliu, D.,

Cortelli, P., et al. (2015). Effect of parasympathetic stimulation on brain activity during appraisal of fearful expressions. Neuropsychopharmacology.

[47] Manning, J. et al. (1975). Hypothalamic modulation of baroreceptor afferent unit activity. American Journal of Physiology– Legacy Content, 229(5):1357–1364.

[48] Martini, N., Menicucci, D., Sebastiani, L., Bedini, R., Pingitore, A., Vanello, N., Milanesi, M., Landini, L., and Gemignani, A. (2012). The dynamics of eeg gamma responses to unpleasant visual stimuli: From local activity to functional connectivity. NeuroImage, 60(2):922–932.

[49] Massari, V. J., Johnson, T. A., and Gatti, P. J. (1995). Cardiotopic organization of the nucleus ambiguus? an anatomical and physiological analysis of neurons regulating atrioventricular conduction. Brain research, 679(2):227–240.

[50] Montano, N., Ruscone, T. G., Porta, A., Lombardi, F., Pagani, M., Malliani, A. (1994). Power spectrum analysis of heart rate variability to assess the changes in sympathovagal balance during graded orthostatic tilt. Circulation, 90(4), 1826-1831.

[51] Muller, M. M., Keil, A., Gruber, T., and Elbert, T. (1999). Processing of affective pictures modulates right-hemispheric gamma band eeg activity. Clinical Neurophysiology, 110(11):1913 – 1920.

[52] Murphy, F. C., Nimmo-Smith, I., and Lawrence, A. D. (2003). Functional neuroanatomy of emotions: a meta-analysis. Cognitive, Affective, & Behavioral Neuroscience, 3(3):207–233.

[53] Oppenheimer, S. (1993). The anatomy and physiology of cortical mechanisms of cardiac control. Stroke, 24(12 Suppl): I3–5.

[54] Oppenheimer, S. M. and Cechetto, D. F. (1990). Cardiac chronotropic organization of the rat insular cortex. Brain research, 533(1):66–72.

[55] Pereira, V. H., Cerqueira, J. J., Palha, J. A., and Sousa, N. (2013). Stressed brain, diseased heart: a review on the pathophysiologic mechanisms of neurocardiology. International journal of cardiology, 166(1):30–37.

[56] Porta, A. and Faes, L. (2016). Wiener–granger causality in network physiology with applications to cardiovascular control and neuroscience. Proceedings of the IEEE, 104(2):282–309.

[57] Posner, J., Russell, J. A., and Peterson, B. S. (2005). The circumplex model of affect: An integrative approach to affective neuroscience, cognitive development, and psychopathology. Development and psychopathology, 17(03):715–734.

[58] Rajendra Acharya, U., Paul Joseph, K., Kannathal, N., Lim, C., and Suri, J. (2006). Heart rate variability: a review. Medical and Biological Engineering and Computing, 44(12):1031–1051.

[59] Sackeim, H. A., Greenberg, M. S., Weiman, A. L., Gur, R. C., Hungerbuhler, J. P., and Geschwind, N. (1982). Hemispheric asymmetry in the expression of positive and negative emotions: neurologic evidence. Archives of neurology,

633 39(4):210–218.

634 [60] Sackeim, H. A., Gur, R. C., and Saucy, M. C. (1978). Emotions are expressed more intensely on the left side of the face.
635 Science, 202(4366):434–436.

636 [61] Saper, C. B. (2002). The central autonomic nervous system: conscious visceral perception and autonomic pattern
637 generation. Annual review of neuroscience, 25(1):433–469

638 [62] Sapru, H. (1991). Spinal mechanisms in the sympathetic control of cardiac function. In Central Neural Mechanisms in
639 Cardiovascular Regulation, pages 183–208. Springer.

640 [63] Sato, W., Kochiyama, T., Yoshikawa, S., Naito, E., and Matsumura, M. (2004). Enhanced neural activity in response to
641 dynamic facial expressions of emotion: an fmri study. Cognitive Brain Research, 20(1):81–91.

642 [64] Saul, J., Berger, R., Albrecht, P., Stein, S., Chen, M., and Cohen, R. (1991). Transfer function analysis of the circulation:
643 unique insights into cardiovascular regulation. American Journal of Physiology-Heart and Circulatory Physiology, 261(4):H1231.

644 [65] Sebastiani, L., Simoni, A., Gemignani, A., Ghelarducci, B., and Santarcangelo, E. (2003). Autonomic and eeg correlates of
645 emotional imagery in subjects with different hypnotic susceptibility. Brain research bulletin, 60(1):151–160.

646 [66] Seth, A. K., Barrett, A. B., and Barnett, L. (2015). Granger causality analysis in neuroscience and neuroimaging. Journal
647 of Neuroscience, 35(8):3293–3297.

648 [67] Silberman, E. K. and Weingartner, H. (1986). Hemispheric lateralization of functions related to emotion. Brain and
649 cognition, 5(3):322–353.

650 [68] Springer, S. P. and Deutsch, G. (1998). Left brain, right brain: Perspectives from cognitive neuroscience. WH
651 Freeman/Times Books/Henry Holt & Co.

652 [69] Sundaram, K., Murugaian, J., Krieger, A., and Sapru, H. (1989a). Microinjections of cholinergic agonists into the
653 intermediolateral cell column of the spinal cord at t1-t3 increase heart rate and contractility. Brain research, 503(1):22–31.

654 [70] Sundaram, K., Murugaian, J., and Sapru, H. (1989b). Cardiac responses to the microinjections of excitatory amino acids
655 into the intermediolateral cell column of the rat spinal cord. Brain research, 482(1):12–22.

656 [71] Taggart, P. and Lambiase, P. (2011). Anger, emotion, and arrhythmias: from brain to heart. Frontiers in physiology, 2:67.

657 [72] Thayer, J. F. and Lane, R. D. (2009). Claude bernard and the heart–brain connection: Further elaboration of a model of
658 neurovisceral integration. Neuroscience & Biobehavioral Reviews, 33(2):81–88.

659 [73] Tokgözoglu, S. L., Batur, M. K., Topuoglu, M. A., Saribas, O., Kes, S., Oto, A. (1999). Effects of stroke localization on
660 cardiac autonomic balance and sudden death. Stroke, 30(7):1307–1311.

661 [74] Tucker, D. M. (1981). Lateral brain function, emotion, and conceptualization. Psychological bulletin, 89(1):19.

[75] Valenza, G., Citi, L., and Barbieri, R. (2014a). Estimation of instantaneous complex dynamics through lyapunov exponents: a study on heartbeat dynamics. PloS one, 9(8):e105622.

[76] Valenza, G., Citi, L., Lanata´, A., Scilingo, E. P., and Barbieri, R. (2014b). Revealing real-time emotional responses: a personalized assessment based on heartbeat dynamics. Scientific reports, 4.

[77] Valenza, G., Citi, L., Scilingo, E. P., and Barbieri, R. (2014c). Inhomogeneous point-process entropy: An instantaneous measure of complexity in discrete systems. Physical Review E, 89(5):052803.

[78] Valenza, G., Greco, A., Gentili, C., Lanata, A., Sebastiani, L., Menicucci, D., Gemignani, A., and Scilingo, E. (2016a). Combining electroencephalographic activity and instantaneous heart rate for assessing brain–heart dynamics during visual emotional elicitation in healthy subjects. Phil. Trans. R. Soc. A, 374(2067):20150176.

[79] Valenza, G., Lanata´, A., and Scilingo, E. P. (2013). Improving emotion recognition systems by embedding cardiorespiratory coupling. Physiological measurement, 34(4):449.

[80] Valenza, G., Toschi, N., and Barbieri, R. (2016b). Uncovering brain-heart information through advanced signal and image processing. Philosophical transactions. Series A, Mathematical, physical, and engineering sciences, 374(2067).

[81] Verberne, A. J. and Owens, N. C. (1998). Cortical modulation of the cardiovascular system. Progress in neurobiology, 54(2):149–168.

[82] Wager, T. D., Phan, K. L., Liberzon, I., and Taylor, S. F. (2003). Valence, gender, and lateralization of functional brain anatomy in emotion: a meta-analysis of findings from neuroimaging. Neuroimage, 19(3):513–531.

[83] Wittling, W., Block, A., Genzel, S., and Schweiger, E. (1998). Hemisphere asymmetry in parasympathetic control of the heart. Neuropsychologia, 36(5):461–468.

[84] Wright, P., He, G., Shapira, N. A., Goodman, W. K., and Liu, Y. (2004). Disgust and the insula: fmri responses to pictures of mutilation and contamination. Neuroreport, 15(15):2347–2351.

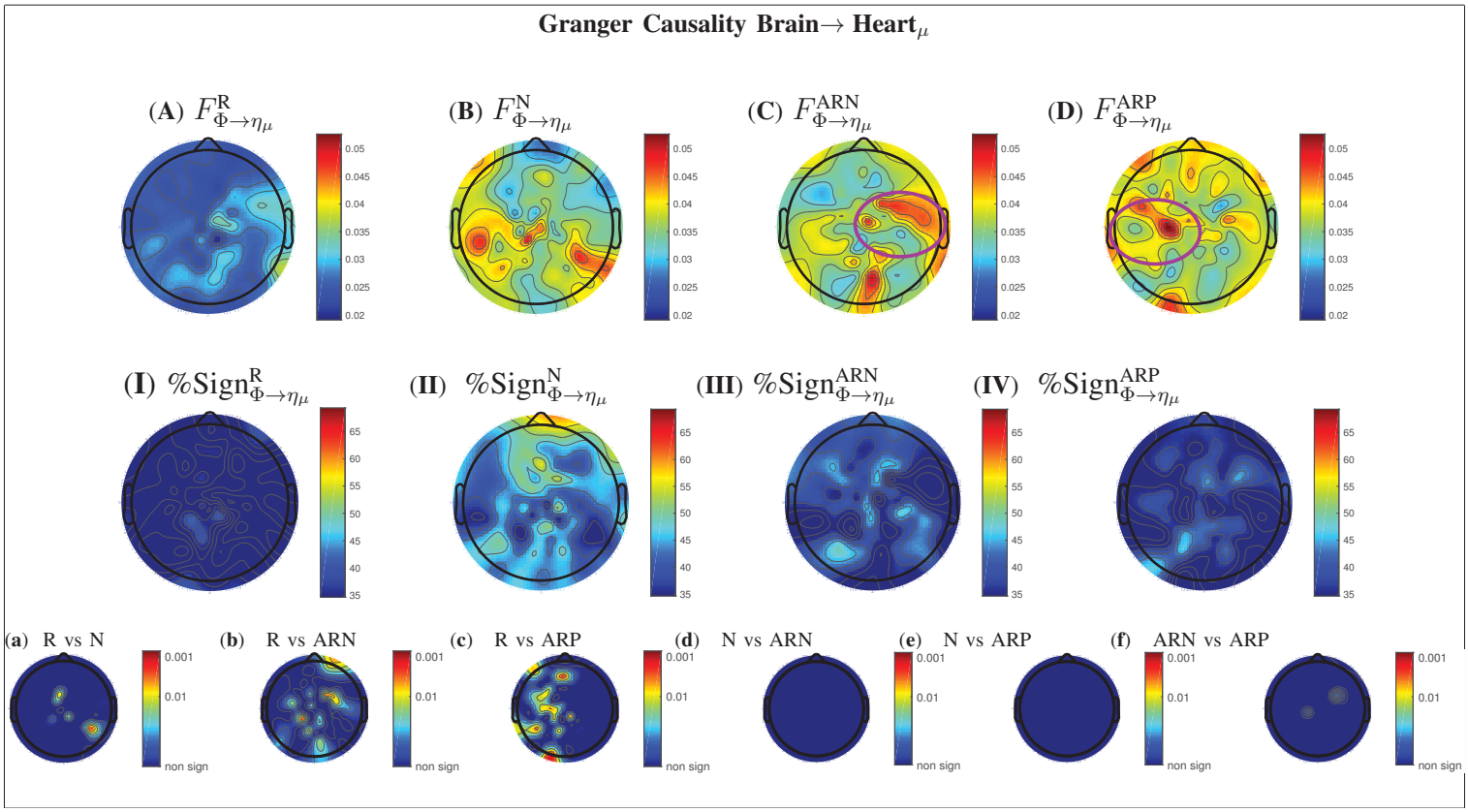
Granger Causality Brain→ Heart$_\mu$
(A) $F^{R}_{\Phi\to\eta_\mu}$
(B) $F^{N}_{\Phi\to\eta_\mu}$
(C) $F^{ARN}_{\Phi\to\eta_\mu}$
(D) $F^{ARP}_{\Phi\to\eta_\mu}$
0.05
0.045
0.04
0.035
0.03
0.025
0.02
(I) %Sign$^{R}_{\Phi\to\eta_\mu}$
(II) %Sign$^{N}_{\Phi\to\eta_\mu}$
(III) %Sign$^{ARN}_{\Phi\to\eta_\mu}$
(IV) %Sign$^{ARP}_{\Phi\to\eta_\mu}$
65
60
55
50
45
40
35
(a) R vs N
(b) R vs ARN
(c) R vs ARP
(d) N vs ARN
(e) N vs ARP
(f) ARN vs ARP
0.001
0.01
non sign

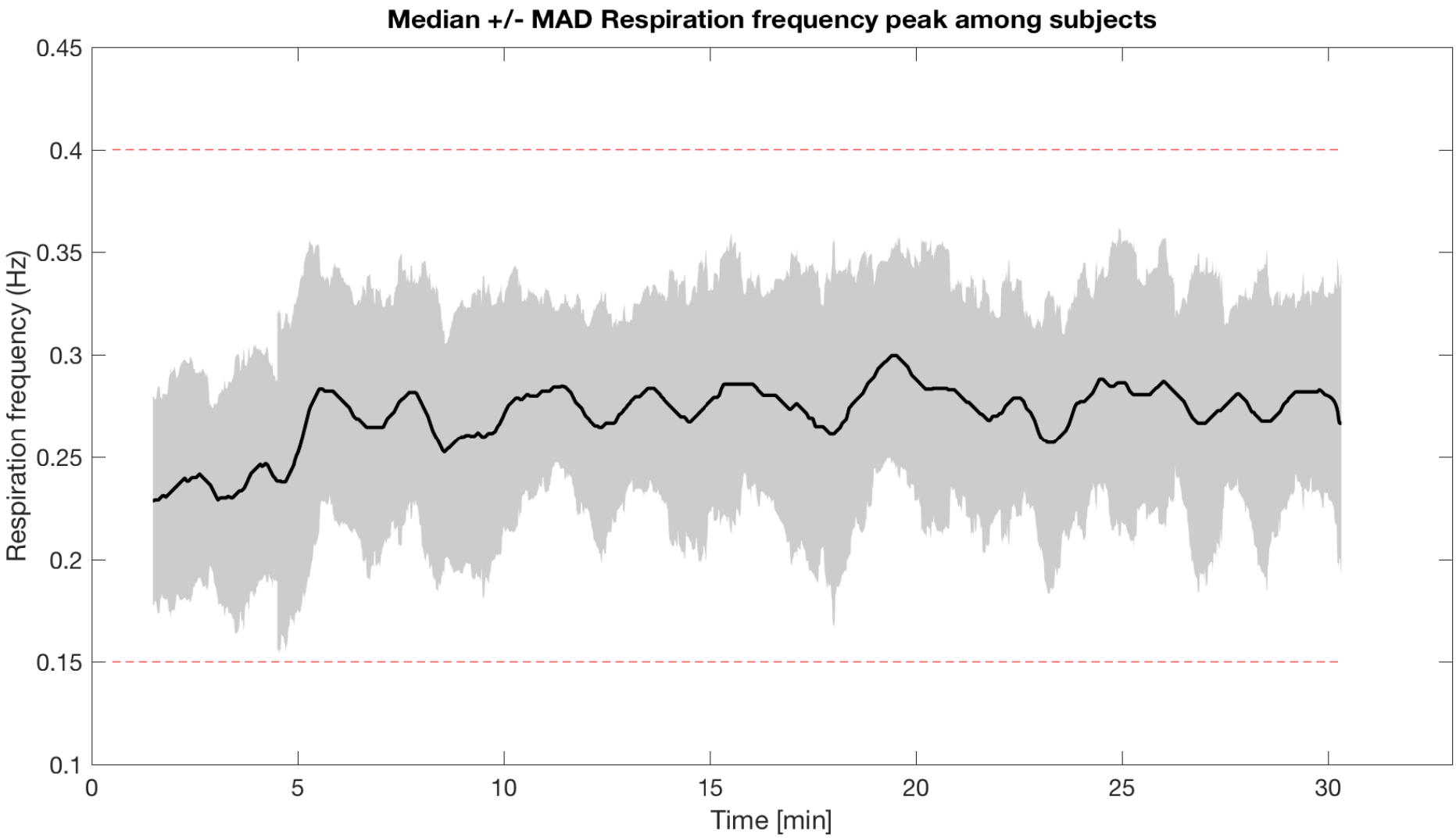
Median +/- MAD Respiration frequency peak among subjects
Respiration frequency (Hz)
0.45
0.4
0.35
0.3
0.25
0.2
0.15
0.1
0
5
10
15
20
25
30
Time [min]

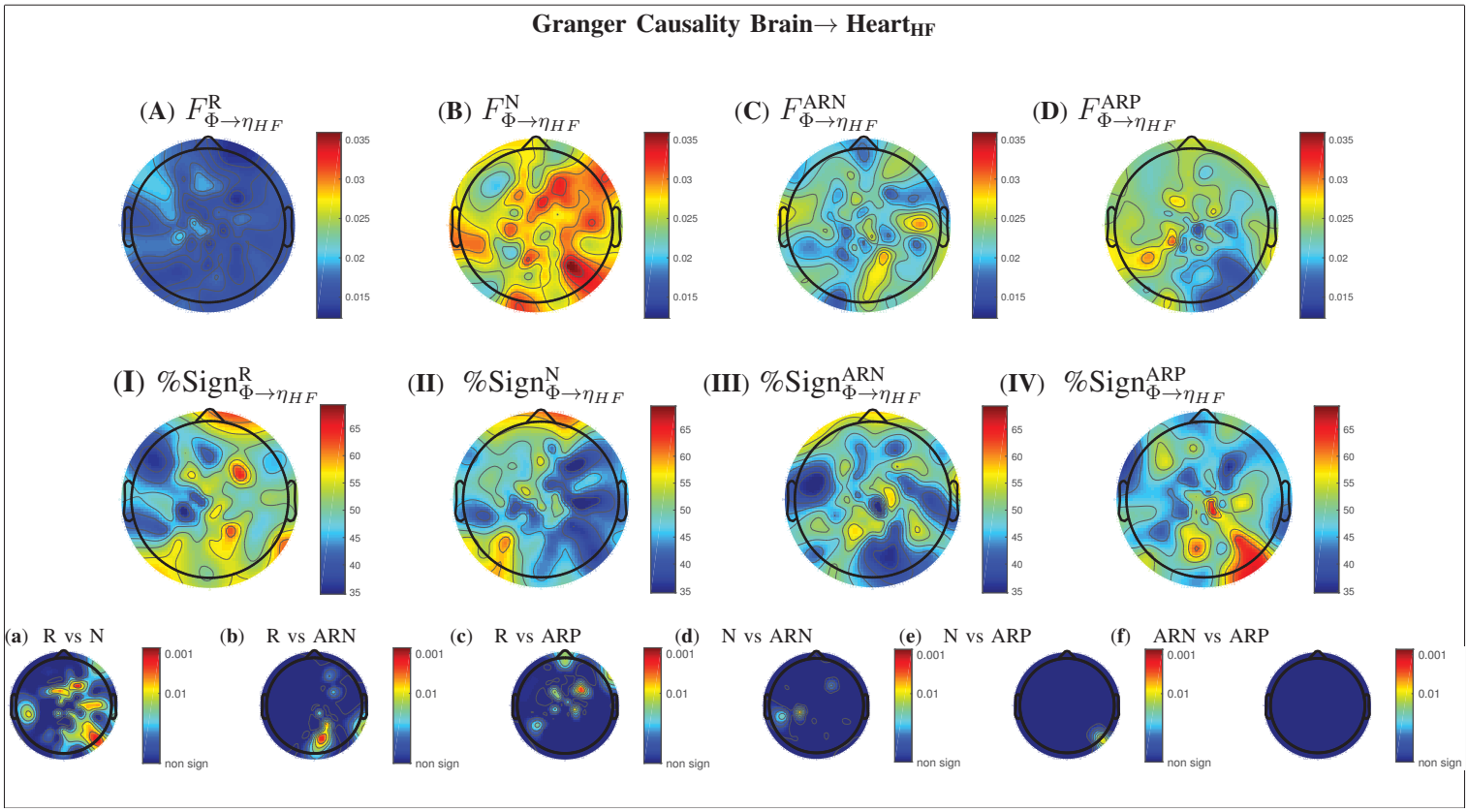
Granger Causality Brain→ Heart$_{\mathbf{HF}}$
(A) $F^{\mathrm{R}}_{\Phi\to\eta_{HF}}$
(B) $F^{\mathrm{N}}_{\Phi\to\eta_{HF}}$
(C) $F^{\mathrm{ARN}}_{\Phi\to\eta_{HF}}$
(D) $F^{\mathrm{ARP}}_{\Phi\to\eta_{HF}}$
0.035
0.03
0.025
0.02
0.015
(I) $\%\mathrm{Sign}^{\mathrm{R}}_{\Phi\to\eta_{HF}}$
(II) $\%\mathrm{Sign}^{\mathrm{N}}_{\Phi\to\eta_{HF}}$
(III) $\%\mathrm{Sign}^{\mathrm{ARN}}_{\Phi\to\eta_{HF}}$
(IV) $\%\mathrm{Sign}^{\mathrm{ARP}}_{\Phi\to\eta_{HF}}$
65
60
55
50
45
40
35
(a) R vs N
(b) R vs ARN
(c) R vs ARP
(d) N vs ARN
(e) N vs ARP
(f) ARN vs ARP
0.001
0.01
non sign

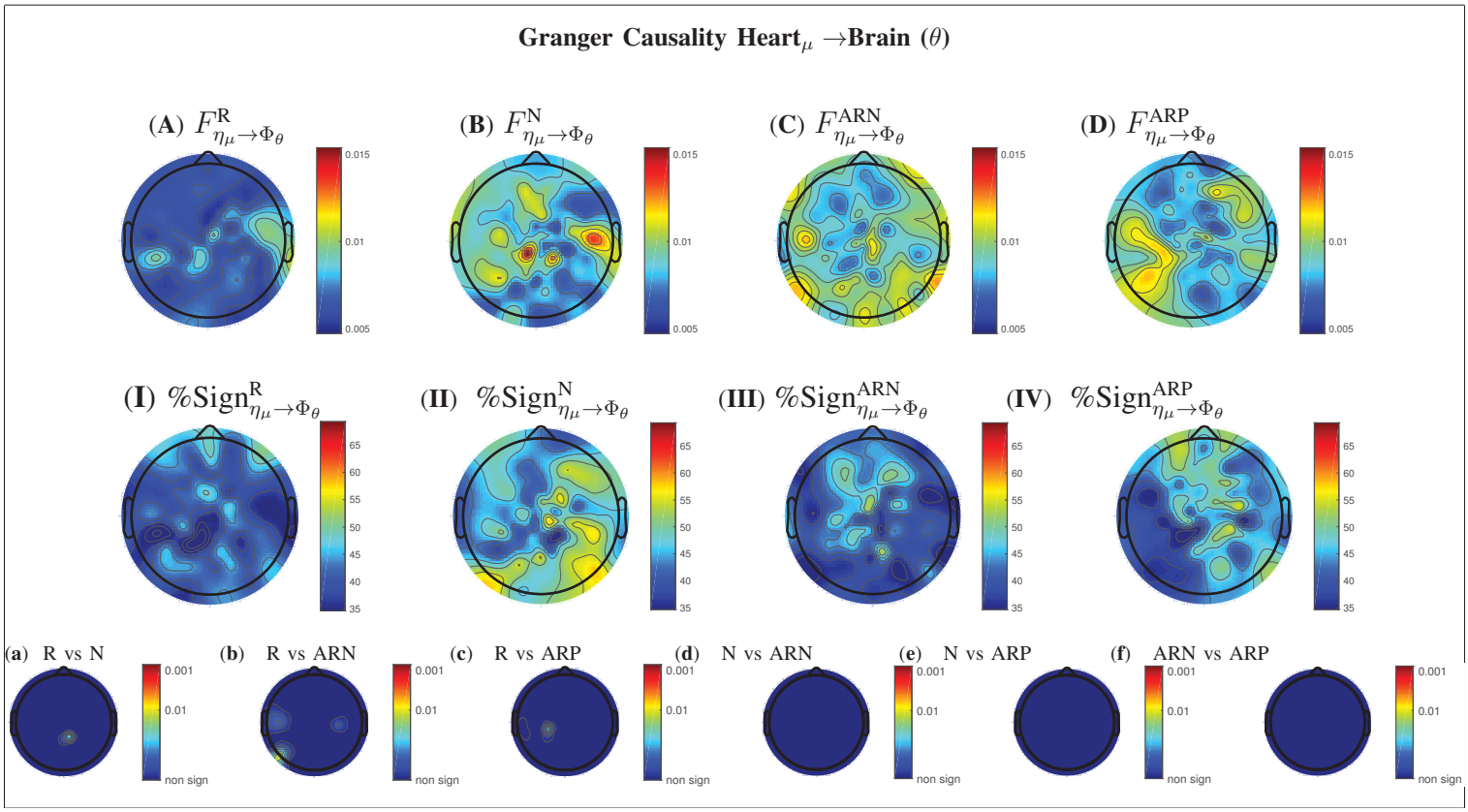
Granger Causality Heart$_\mu$ →Brain (θ)
(A) $F^{R}_{\eta_\mu \to \Phi_\theta}$
(B) $F^{N}_{\eta_\mu \to \Phi_\theta}$
(C) $F^{ARN}_{\eta_\mu \to \Phi_\theta}$
(D) $F^{ARP}_{\eta_\mu \to \Phi_\theta}$
0.015
0.01
0.005
(I) %Sign$^{R}_{\eta_\mu \to \Phi_\theta}$
(II) %Sign$^{N}_{\eta_\mu \to \Phi_\theta}$
(III) %Sign$^{ARN}_{\eta_\mu \to \Phi_\theta}$
(IV) %Sign$^{ARP}_{\eta_\mu \to \Phi_\theta}$
65
60
55
50
45
40
35
(a) R vs N
(b) R vs ARN
(c) R vs ARP
(d) N vs ARN
(e) N vs ARP
(f) ARN vs ARP
0.001
0.01
non sign

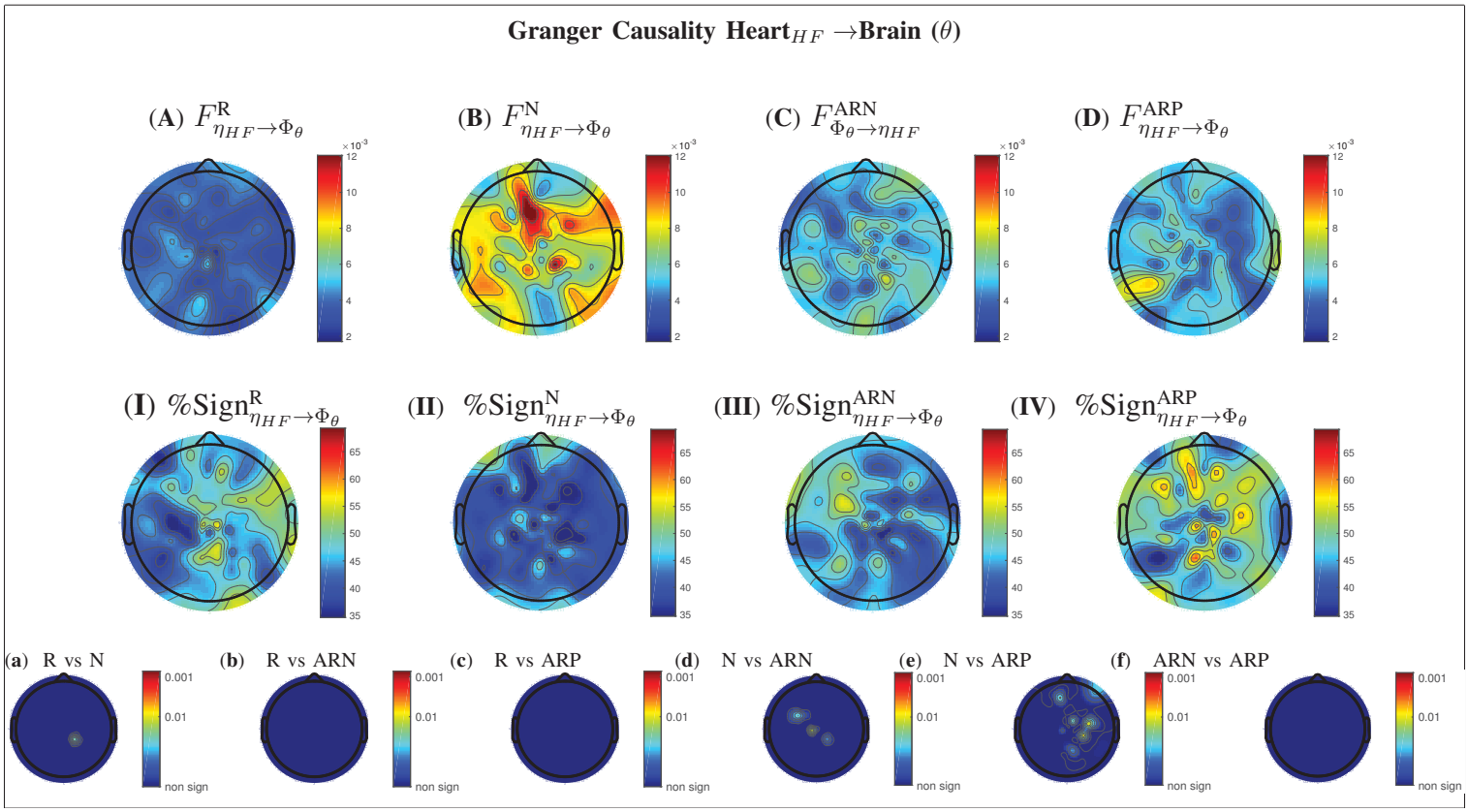
Granger Causality Heart$_{HF}$ →Brain (θ)
(A) $F^{R}_{\eta_{HF}\to\Phi_\theta}$
(B) $F^{N}_{\eta_{HF}\to\Phi_\theta}$
(C) $F^{ARN}_{\Phi_\theta\to\eta_{HF}}$
(D) $F^{ARP}_{\eta_{HF}\to\Phi_\theta}$
(I) %Sign$^{R}_{\eta_{HF}\to\Phi_\theta}$
(II) %Sign$^{N}_{\eta_{HF}\to\Phi_\theta}$
(III) %Sign$^{ARN}_{\eta_{HF}\to\Phi_\theta}$
(IV) %Sign$^{ARP}_{\eta_{HF}\to\Phi_\theta}$
(a) R vs N
(b) R vs ARN
(c) R vs ARP
(d) N vs ARN
(e) N vs ARP
(f) ARN vs ARP
0.001
0.01
non sign

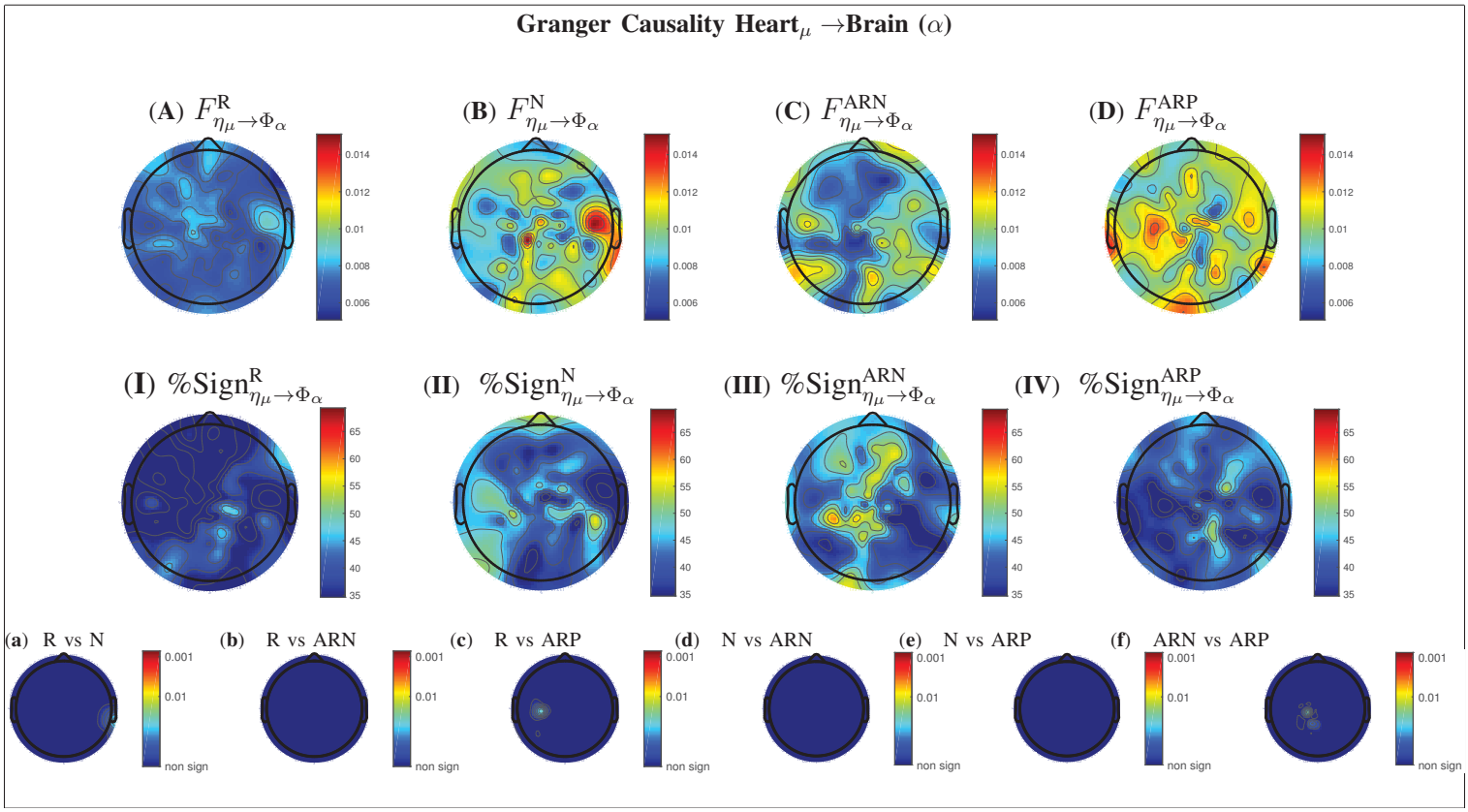
Granger Causality Heart$_\mu$ →Brain (α)
(A) $F^{R}_{\eta_\mu \to \Phi_\alpha}$
(B) $F^{N}_{\eta_\mu \to \Phi_\alpha}$
(C) $F^{ARN}_{\eta_\mu \to \Phi_\alpha}$
(D) $F^{ARP}_{\eta_\mu \to \Phi_\alpha}$
0.014
0.012
0.01
0.008
0.006
(I) %Sign$^{R}_{\eta_\mu \to \Phi_\alpha}$
(II) %Sign$^{N}_{\eta_\mu \to \Phi_\alpha}$
(III) %Sign$^{ARN}_{\eta_\mu \to \Phi_\alpha}$
(IV) %Sign$^{ARP}_{\eta_\mu \to \Phi_\alpha}$
65
60
55
50
45
40
35
(a) R vs N
(b) R vs ARN
(c) R vs ARP
(d) N vs ARN
(e) N vs ARP
(f) ARN vs ARP
0.001
0.01
non sign

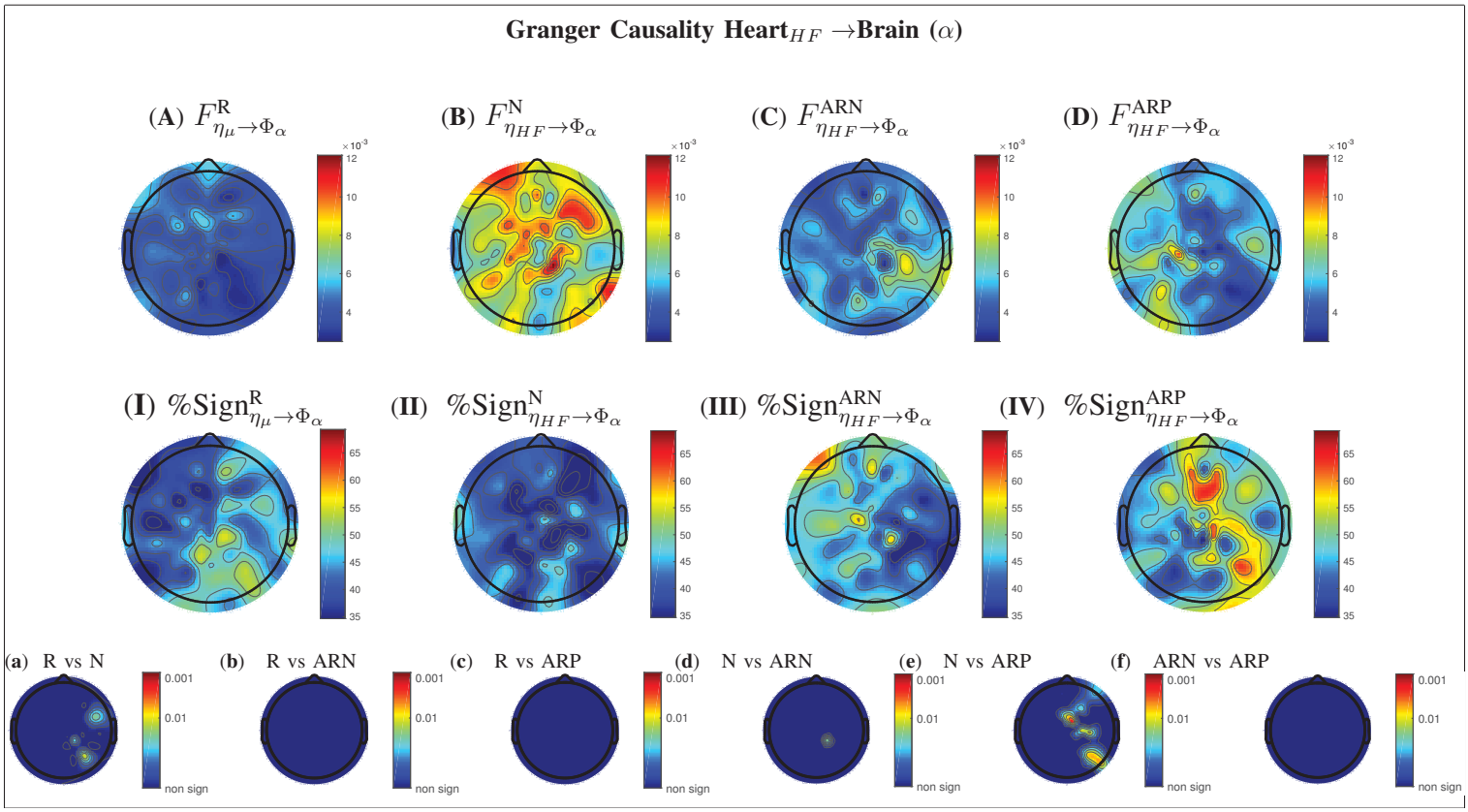
Granger Causality Heart$_{HF}$ →Brain (α)
(A) $F^{R}_{\eta_\mu \to \Phi_\alpha}$
(B) $F^{N}_{\eta_{HF} \to \Phi_\alpha}$
(C) $F^{ARN}_{\eta_{HF} \to \Phi_\alpha}$
(D) $F^{ARP}_{\eta_{HF} \to \Phi_\alpha}$
×10^-3
12
10
8
6
4
(I) %Sign$^{R}_{\eta_\mu \to \Phi_\alpha}$
(II) %Sign$^{N}_{\eta_{HF} \to \Phi_\alpha}$
(III) %Sign$^{ARN}_{\eta_{HF} \to \Phi_\alpha}$
(IV) %Sign$^{ARP}_{\eta_{HF} \to \Phi_\alpha}$
65
60
55
50
45
40
35
(a) R vs N
(b) R vs ARN
(c) R vs ARP
(d) N vs ARN
(e) N vs ARP
(f) ARN vs ARP
0.001
0.01
non sign

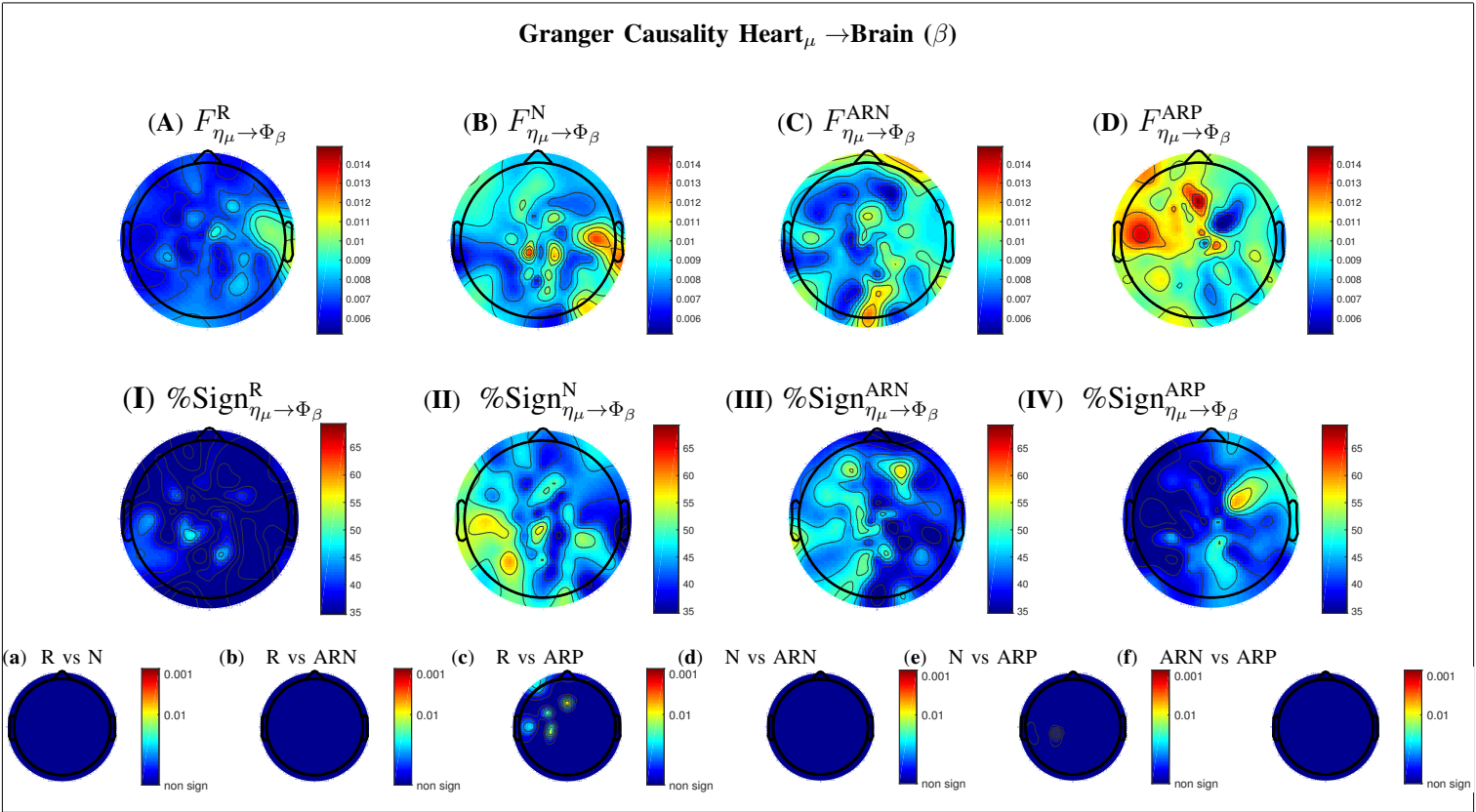
Granger Causality Heart$_\mu$ →Brain (β)
(A) $F^{R}_{\eta_\mu \to \Phi_\beta}$
(B) $F^{N}_{\eta_\mu \to \Phi_\beta}$
(C) $F^{ARN}_{\eta_\mu \to \Phi_\beta}$
(D) $F^{ARP}_{\eta_\mu \to \Phi_\beta}$
0.014
0.013
0.012
0.011
0.01
0.009
0.008
0.007
0.006
(I) $\%Sign^{R}_{\eta_\mu \to \Phi_\beta}$
(II) $\%Sign^{N}_{\eta_\mu \to \Phi_\beta}$
(III) $\%Sign^{ARN}_{\eta_\mu \to \Phi_\beta}$
(IV) $\%Sign^{ARP}_{\eta_\mu \to \Phi_\beta}$
65
60
55
50
45
40
35
(a) R vs N
(b) R vs ARN
(c) R vs ARP
(d) N vs ARN
(e) N vs ARP
(f) ARN vs ARP
0.001
0.01
non sign

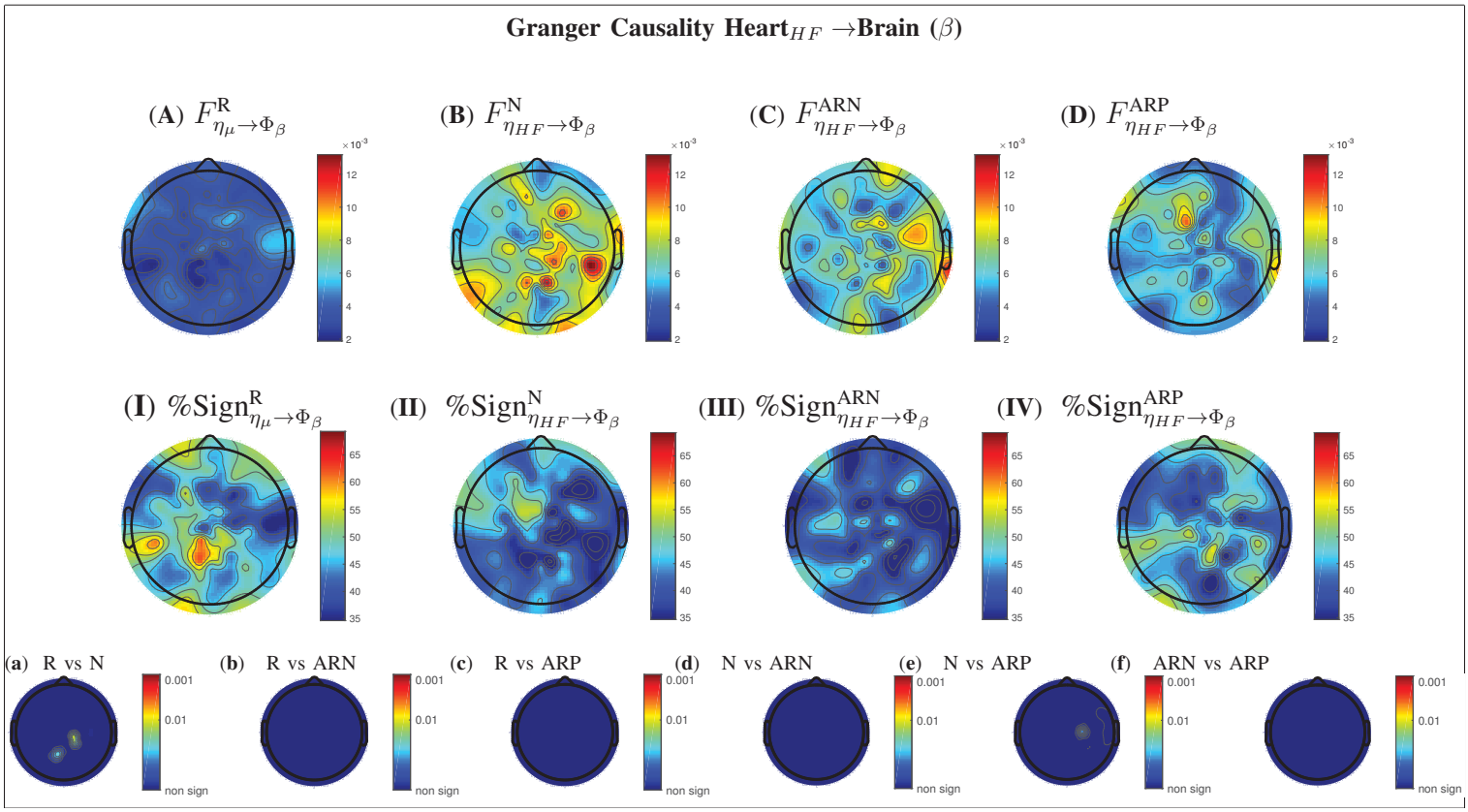
Granger Causality Heart$_{HF}$ →Brain (β)
(A) $F^{R}_{\eta_\mu \to \Phi_\beta}$
(B) $F^{N}_{\eta_{HF} \to \Phi_\beta}$
(C) $F^{ARN}_{\eta_{HF} \to \Phi_\beta}$
(D) $F^{ARP}_{\eta_{HF} \to \Phi_\beta}$
(I) %Sign$^{R}_{\eta_\mu \to \Phi_\beta}$
(II) %Sign$^{N}_{\eta_{HF} \to \Phi_\beta}$
(III) %Sign$^{ARN}_{\eta_{HF} \to \Phi_\beta}$
(IV) %Sign$^{ARP}_{\eta_{HF} \to \Phi_\beta}$
(a) R vs N
(b) R vs ARN
(c) R vs ARP
(d) N vs ARN
(e) N vs ARP
(f) ARN vs ARP
0.001
0.01
non sign

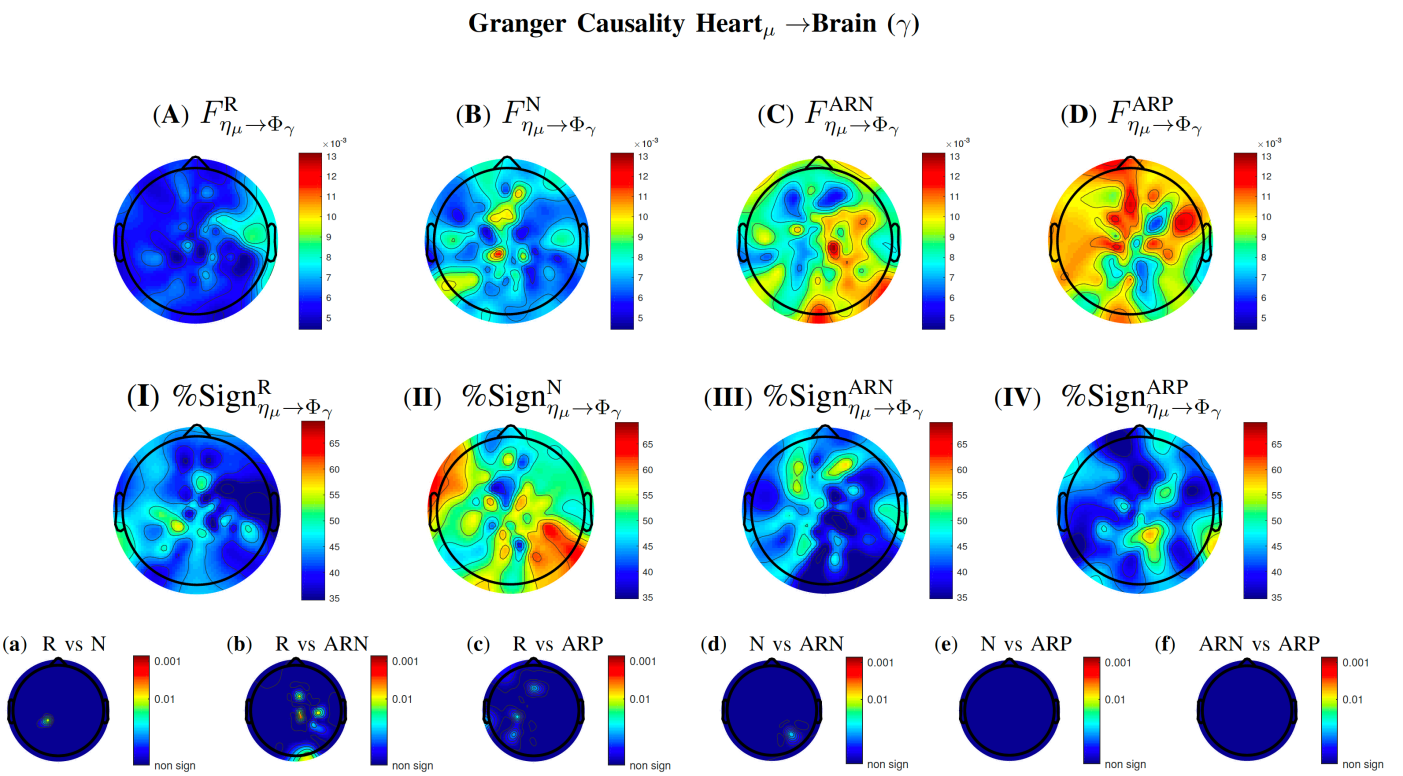
Granger Causality Heart$_\mu$ →Brain (γ)
(A) $F^{R}_{\eta_\mu \to \Phi_\gamma}$
(B) $F^{N}_{\eta_\mu \to \Phi_\gamma}$
(C) $F^{ARN}_{\eta_\mu \to \Phi_\gamma}$
(D) $F^{ARP}_{\eta_\mu \to \Phi_\gamma}$
×10^-3
13
12
11
10
9
8
7
6
5
(I) %Sign$^{R}_{\eta_\mu \to \Phi_\gamma}$
(II) %Sign$^{N}_{\eta_\mu \to \Phi_\gamma}$
(III) %Sign$^{ARN}_{\eta_\mu \to \Phi_\gamma}$
(IV) %Sign$^{ARP}_{\eta_\mu \to \Phi_\gamma}$
65
60
55
50
45
40
35
(a) R vs N
(b) R vs ARN
(c) R vs ARP
(d) N vs ARN
(e) N vs ARP
(f) ARN vs ARP
0.001
0.01
non sign

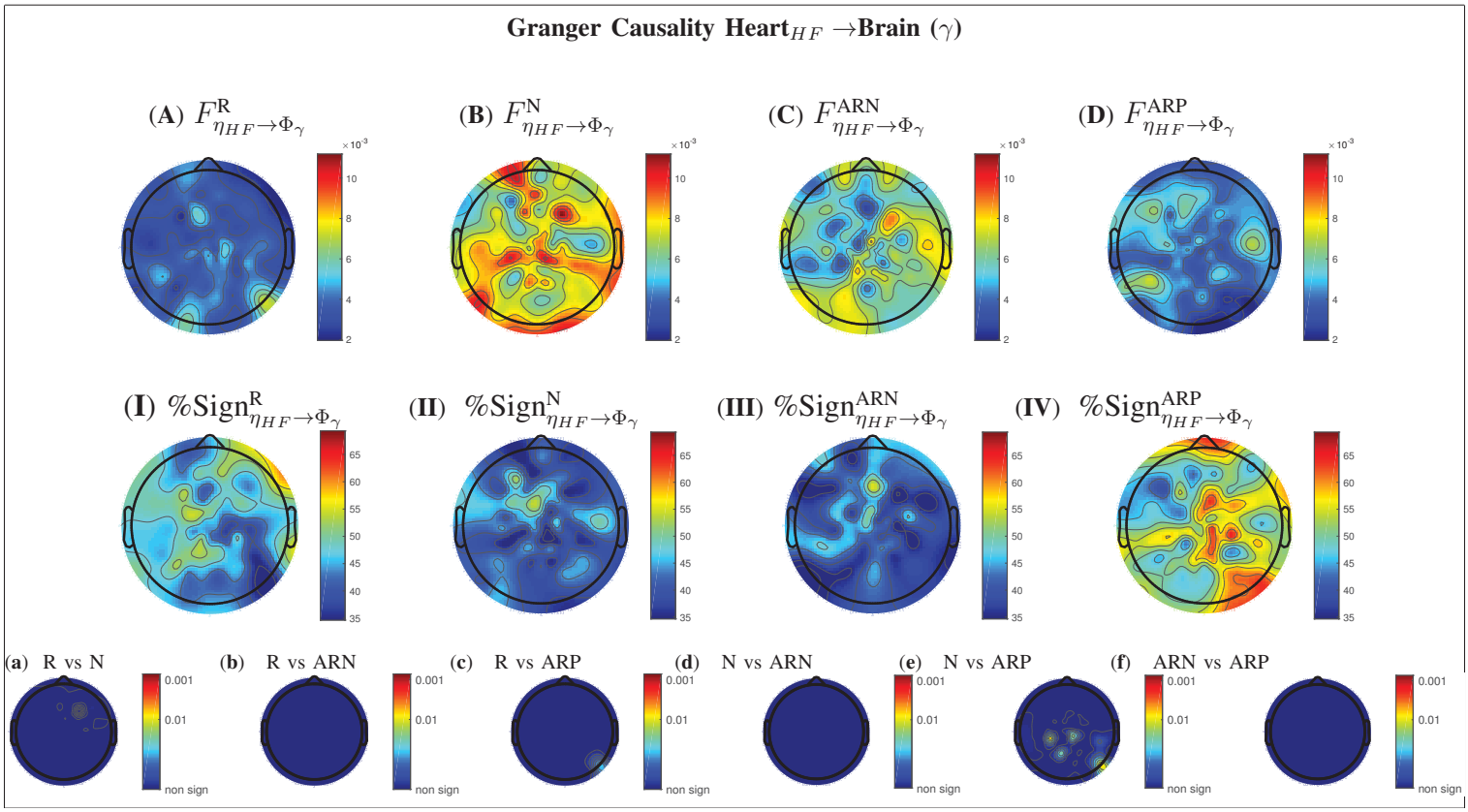
Granger Causality Heart$_{HF}$ →Brain (γ)
(A) $F^{R}_{\eta_{HF}\to\Phi_\gamma}$
(B) $F^{N}_{\eta_{HF}\to\Phi_\gamma}$
(C) $F^{ARN}_{\eta_{HF}\to\Phi_\gamma}$
(D) $F^{ARP}_{\eta_{HF}\to\Phi_\gamma}$
×10^-3
10
8
6
4
2
(I) %Sign$^{R}_{\eta_{HF}\to\Phi_\gamma}$
(II) %Sign$^{N}_{\eta_{HF}\to\Phi_\gamma}$
(III) %Sign$^{ARN}_{\eta_{HF}\to\Phi_\gamma}$
(IV) %Sign$^{ARP}_{\eta_{HF}\to\Phi_\gamma}$
65
60
55
50
45
40
35
(a) R vs N
(b) R vs ARN
(c) R vs ARP
(d) N vs ARN
(e) N vs ARP
(f) ARN vs ARP
0.001
0.01
non sign